Henry Whittington

Design of Shaped Charges

University of Wales Trinity Saint David, School of Applied Computing
Ordnance, Munitions and Explosives

BEng
Academic Year: 2025 - 2026

Supervisor: Prof. Kelvin Donne

Academic integrity declaration

I declare that:

- the thesis submitted has been written by me alone.
- the thesis submitted has not been previously submitted to this university or any other.
- that all content, including primary and/or secondary data, is true to the best of my knowledge.
- that all quotations and references have been duly acknowledged according to the requirements of academic research.

I understand that to knowingly submit work in violation of the above statement will be considered by examiners as academic misconduct.

Abstract

Shaped charge systems are widely utilised in the modern defence, petroleum, mining and demolition industries and are therefore the subject of extensive research into design factors and potential applications of new metallurgical and energetics technology.

This essay reviews modern scientific literature on shaped charge design in order to create three digital models of a shaped charge system. Simulations are then run with these models and the results analysed.

The results show a broad agreement with published literature, although some areas could not be fully explored due to time and computing constraints.

Keywords:

Abaqus CAE, shaped charge, blast modelling, Johnson-Cook, Jones Wilkins & Lee, equations of state

Table of Contents

Academic integrity declaration i
Abstract ii
List of Figures v
List of Tables vii
List of Equations viii
List of Abbreviations ix
1 Shaped Charges 10
1.1 The Shaped Charge System 10
1.2 The History of Shaped Charges 10
1.3 Modern Shaped Charge Use 11
1.4 Military Shaped Charges 13
2 Shaped Charge Design Factors 14
2.1 Liner Shape 14
2.2 Liner Angle 15
2.3 Liner Material 16
2.4 Explosive Composition 16
3 Shaped Charge Modelling 18
3.1 Shaped Charge Design Parameters 18
3.2 Shaped Charge System Design 19
3.2.1 System Restrictions 19
3.2.2 Liner Parameters 19
3.2.3 Casing Parameters 19
3.2.4 Materials Used 20
4 2D shaped charge construction in Abaqus 21
4.1 Geometry 21
4.2 Materials and equations of state 21
4.3 Boundary conditions and detonation point 24
4.4 Meshing 24
5 3D shaped charge construction in Abaqus 28
5.1 Geometry 28
5.2 Boundary conditions and detonation point 28
5.3 Materials and equations of state 30
5.4 Meshing 30
5.5 Dynamic remeshing and smooth particle hydrodynamics 34
5.5.1 Dynamic remeshing 35
5.5.2 Smooth particle hydrodynamics 37
6 Results 38
6.1 System A (copper liner) 38
6.1.1 Velocity 38
6.1.2 Pressure 40

6.1.3 Maximum principal stress 43
6.2 System B 45
6.2.1 Velocity 45
6.2.2 Pressure and stress 47
6.3 3D simulation 48
6.3.1 Velocity 48
6.4 3D simulation (SPH) 50
6.4.1 Velocity 50
7 Discussion 52
7.1.1 Velocity (System A and System B) 52
7.1.2 Velocity (3D simulation) 54
8 Conclusion 56
9 Bibliography 57

List of Figures

Figure 1 - An anti-tank rocket containing a simple shaped charge system..... 10

Figure 2 - A series of shaped charges used in oil well perforation 12

Figure 3 - A linear cutting charge 13

Figure 4 - Some shaped charge liner shapes..... 14

Figure 5 - Shaped charge jet formation dependent on liner cone angle 15

Figure 8 - 2D model of the shaped charge system..... 21

Figure 9 - Material sections created in Abaqus 23

Figure 10 - 2D model of the shaped charge system with boundary conditions shown on the lower edge..... 24

Figure 11 - Detail of the mesh for the 2D model, showing the section where the explosive fill meets the base of the liner 25

Figure 12 - Screenshot showing the distorted elements in early simulations (highlighted in red)..... 26

Figure 13 - The final mesh for the 2D model 27

Figure 14 – Initial 3D model of the shaped charge system..... 28

Figure 15 - Boundary conditions applied to the 3D model..... 29

Figure 16 - Materials and equations of state used (3D model)..... 30

Figure 17 - Elements excessively deformed during the 3D simulation (highlighted in red) 31

Figure 18 - The final mesh for the 3D model 32

Figure 19 - Detail of the mesh graduation, showing the matching of element sizes along the charge/liner border..... 33

Figure 20 - The 3D model used in SPH and ALE simulations, showing the smaller sections created 35

Figure 21 - ALE settings used for the 3D simulation 36

Figure 22 - ALE surface interactions 36

Figure 23 - SPH settings used for 3D simulation..... 37

Figure 24 - Nodes selected at the base of the copper liner 38

Figure 25 - Velocity of the shaped charge liner (System A) 40

Figure 26 – Pressure wave within System A (t=1.0033E-06 s) 41

Figure 27 - Pressure wave within System A (t=3.8015E-06 s) 41
Figure 28 - Pressure wave within System A (t=8.5E-06 s) 42
Figure 29 - Pressure wave within System A (t=1.2E-06 s) 43
Figure 30 - Max principal stress within System A (t=1.2E-05 s) 43
Figure 31 - Nodes selected at the base of the titanium liner 45
Figure 32 - Velocity of the shaped charge liner (System B) 47
Figure 33 - Nodes selected at the base of the 3D liner 48
Figure 34 - Velocity of the shaped charge liner (3D) 50
Figure 35 - Velocity of the shaped charge jet (3D simulation) 54

List of Tables

Table 1 - Shaped charge liner dimensions 19
Table 2 - Shaped charge system casing dimensions 20
Table 3 - Shaped charge system materials 20
Table 4 - Materials and equations of state used (2D model) 22
Table 5 - Johnson-Cook properties used 23
Table 6 - Jones, Wilkins & Lee properties used 23
Table 7 - Observed jet tip velocity 53
Table 8 - Key material differences between copper and titanium 53

List of Equations

Equation 1 - The Johnson-Cook model 21

Equation 2 - The Jones, Wilkins & Lee model 22

List of Abbreviations

ALE	Arbitrary Lagrangian Eularian
SPH	Smooth Particle Hydrodynamics

1 Shaped Charges

1.1 The Shaped Charge System

A shaped charge system consists of an explosive charge and a metallic liner, contained within a case [1]. On detonation of the charge, the pressures created within the case force the metallic liner into a ‘jet’, which is propelled at high speed into a target, causing significant damage.

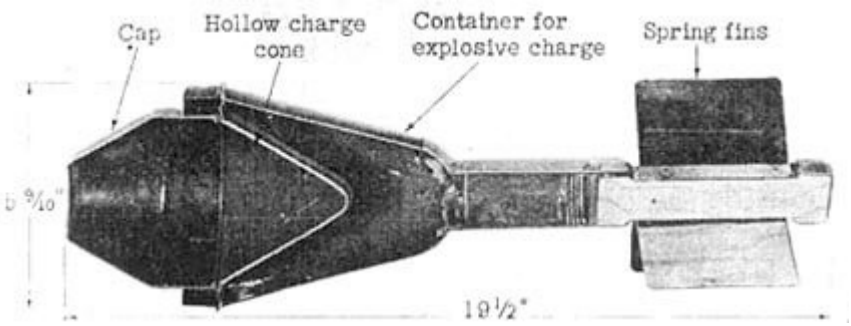

Figure 1 - An anti-tank rocket containing a simple shaped charge system

1.2 The History of Shaped Charges

Although experiments on ‘hollow’ charges, making use of opposing detonation waves to increase the power of a hemispherical explosive charge, had been conducted as early as the late 1700s [2], it was not until the late 1800s that the ‘Munro Effect’ was demonstrated, showing how these opposing waves can form a charge liner into a high velocity jet capable of penetrating steel plate [2].

Military applications of the shaped charge did not appear until the middle of the Second World War, when improvements in tank armour made simple kinetic energy penetration of armoured vehicles more difficult [3]. The first shaped charge weapons, such as the German ‘Panzerfaust’ and the American Bazooka rocket, showed that shaped charge munitions effective against armour could be significantly lighter and more portable than other anti-armour weapons of the time [3].

During the Second World War, all major nations continued to research improved shaped charge munitions, although this research was slowed by material restraints and a wartime emphasis on production of proven weapons over

development of experimental models. Post-war, with fewer restraints, shaped charge munitions development increased from simple man-portable anti-tank munitions and artillery shells to guided missile systems utilising shaped charge warheads [4].

By the late 1980s, shaped charge design had been refined to the point where a handbook for their design had been published [5], and a wide variety of shaped charge munitions, from man-portable anti tank rockets to wire-guided anti-tank missiles, were in service with every major country [4].

Modern research on shaped charges continues to explore the influence of liner shape, liner material, charge energetics and stand-off distance on shaped charge performance.

1.3 Modern Shaped Charge Use

Shaped charges are widely used within the petroleum [6], mining [7] [8], defence [4] and demolition [9] [8] industries. The requirements within each area, and therefore the form of the charges used, vary significantly.

Shaped charges are used within the mining and petroleum industries to blast cavities within subterranean rock [6] [8], often using dozens of charges at one time. Shaped charge designs for the mining industry are therefore influenced by the short standoff distances afforded by close contact with the rock, as well as the challenges faced by firing several charges in close contact with one another.

Shaped charge designs for military applications must balance lethality (the speed and mass of the jet) with reliability and portability. As military shaped charge systems are often used in a man-portabile anti-armour role [4] [10], size and weight must be kept within strict limits to allow portability, without sacrificing reliability or effectiveness. The design of an efficient shaped charge system is therefore paramount to ensure that the limited size and weight is fully utilized.

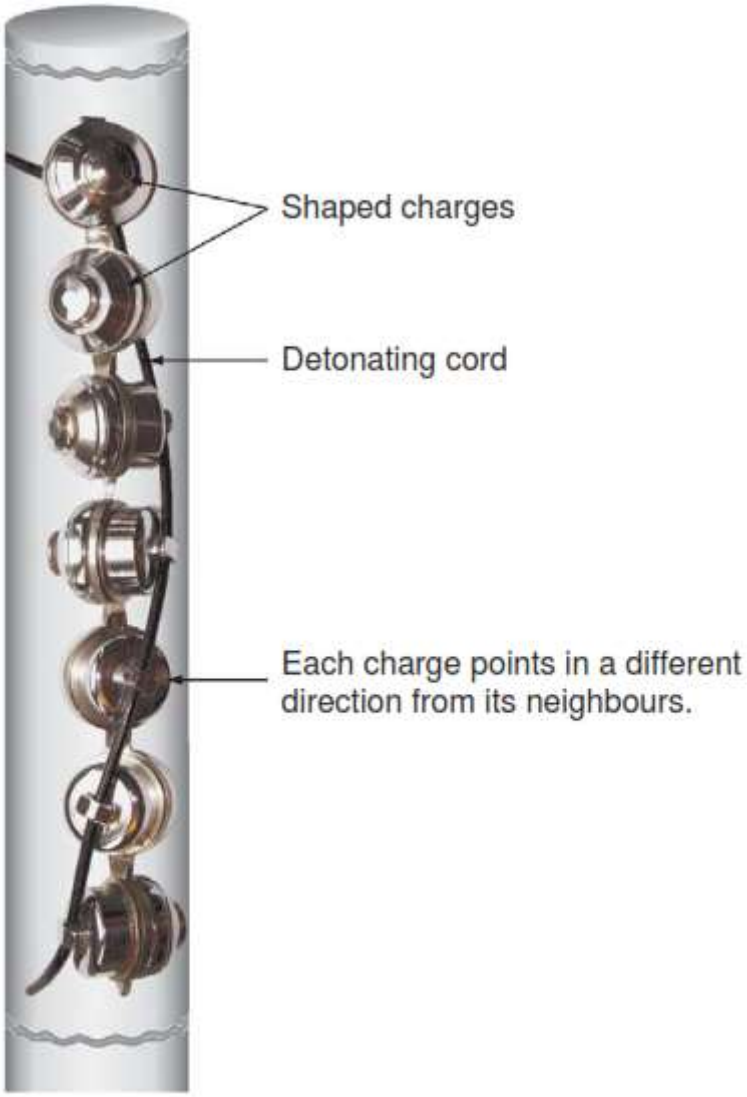

Figure 2 - A series of shaped charges used in oil well perforation

Shaped charges are used within the demolition industry primarily to cut sctructural supports [8], such as beams or columns. They therefore utilise a longer bar-shaped liner, rather than the more common conical liner, to create this cutting effect on the target surface [11].

Figure 3 - A linear cutting charge

1.4 Military Shaped Charges

This essay will focus on the military applications and requirements of shaped charge systems. As mentioned above, a shaped charge system for military purposes must fit within a strict set of size, weight and other limitations in order to either remain man-portable, or to interface correctly with a platform such as a vehicle or aircraft.

Shaped charge systems used within weapons are intended to defeat the armour plating of vehicles [4] [10], as such systems offer a similar armour piercing capability to kinetic energy weapons while offering increased portability and guidance opportunities.

The performance of a shaped charge system in a military context is generally measured by the depth of penetration through steel which can be achieved by a certain design. In order to achieve the maximum depth of penetration within a certain set of restraints, extensive research has been undertaken to understand the impact of various design choices on the armour penetration capabilities of a shaped charge system.

2 Shaped Charge Design Factors

2.1 Liner Shape

This refers to the geometric shape and thickness of the shaped charge liner. While military shaped charge systems favour a conical liner, which produces a cylindrical penetration effect [12], research has compared conical, biconical, elliptical (or trumpet shaped), and ellipsoid liner shapes [13].

Through both live firings and digital modelling, the performance of each lner shape has been assessed. Studies [13] [14] have shown an increase in jet tip velocity using a 'trumpet' shaped liner, which led to an increase in penetration depth compared to both conical and elliptical liners.

Research has also been undertaken to assess the effect of liner thickness on the velocity of the shaped charge jet, comparing uniform liner thickness with progressive thickness. One report [13] suggests that a thinner liner provides a higher jet tip velocity, while a thicker liner produce a longer jet.

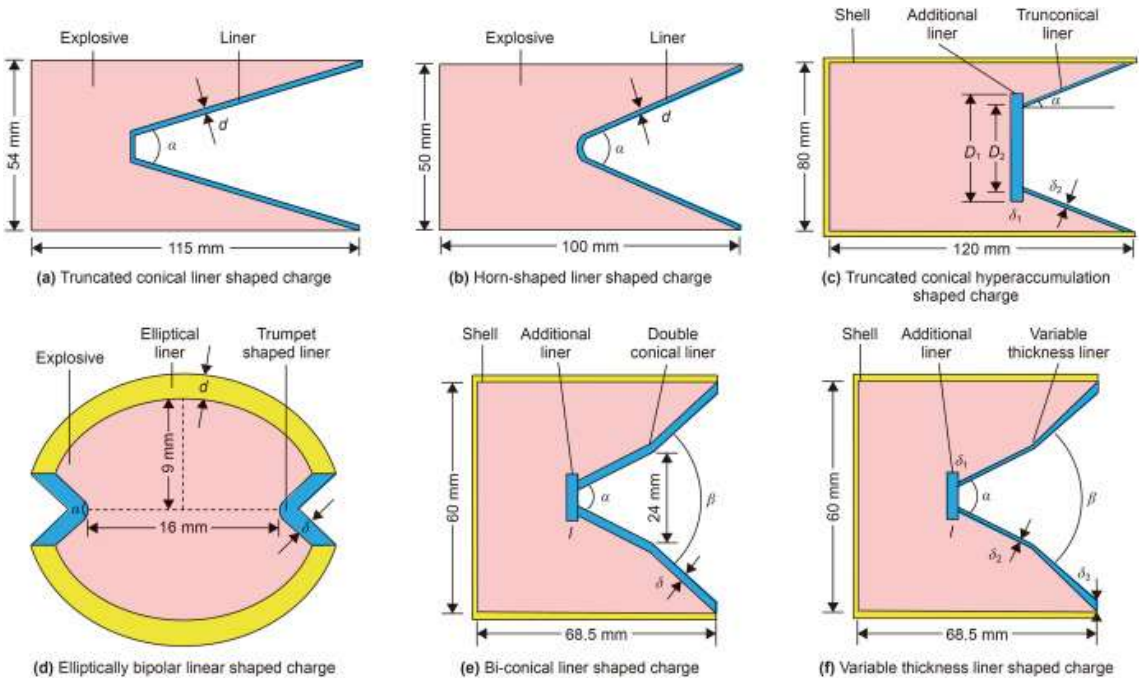

Figure 4 - Some shaped charge liner shapes

Experiments have also been carried out to determine the effect of a ‘grooved’ conical liner with ridges cut into the target-facing front of the liner [15], although the experimental data showed that these grooves did not significantly affect the velocity of the jet.

While the improved performance of novel liner geometries has been demonstrated experimentally [13] [14], questions remain whether the improved efficacy of these designs justifies the increased manufacturing complexity [16] while simpler liner geometries remain effective in the modern battlespace [17].

2.2 Liner Angle

Research has shown that shaped charge liners with narrower angle form a longer jet, while a wider liner angle results in a larger ‘slug’ of metal at the tail of the jet [13] [3]. At extremely shallow angles, an explosive shockwave applied to the liner ceases to produce a hydrodynamic jet and instead propels the liner entirely as a ballistic slug [18].

Such ‘explosively formed projectiles’ are less effective at defeating armour than a shaped charge jet, yet can be found as components in many military systems [19] [20].

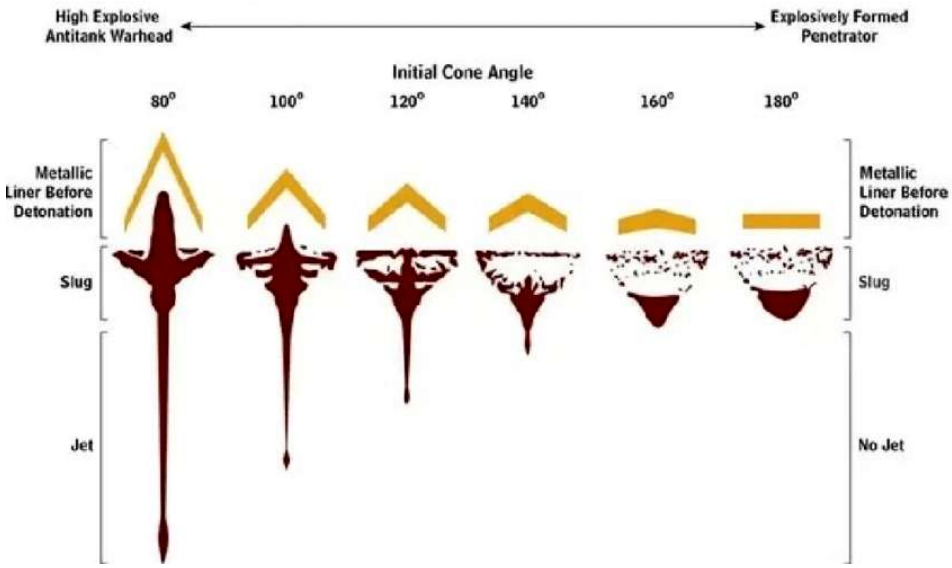

Figure 5 - Shaped charge jet formation dependent on liner cone angle

2.3 Liner Material

The performance of a shaped charge system is heavily dependent on the interactions between the explosive shockwave and the metallic liner [3], and these interactions are greatly influenced by the material properties of the liner.

While copper has been accepted as the standard shaped charge liner for the majority of military applications [1] [3], significant research is ongoing to determine the merits of various metals as shaped charge liners [21].

Some materials have the requisite material properties to be an effective shaped charge liner, but possess other qualities which make them undesirable for widespread use. An example of these is depleted Uranium, which although safe to handle in its solid state produces highly toxic residues when exposed to the temperatures and pressures of a high explosive detonation [22].

Novel shaped charge designs attempt to balance suitability of materials against the costs involved with mass production – while certain metals, such as gold [23] and tungsten [24], are theoretically suitable as shaped charge liners, the costs of raw materials and complexity of manufacturing preclude these from use in all but the most niche designs. However, experiments with copper alloys [25] [26] have shown an increase in performance compared to pure copper liners.

2.4 Explosive Composition

As with liner materials and geometries, the development of shaped charge systems must balance the efficacy of the system against ease and cost of manufacture. Where explosive compositions are concerned, stability and reliability must also be considered [5] [27]. Composition selection may also be influenced by the requirements of the wider system, such as insensitive munitions requirements [28].

Typically, shaped charge systems utilize well understood high explosives with a high detonation velocity [29] [3], such as HMX or RDX, with research exploring different compositions of HMX/TNT [27] and RDX/TNT [30].

Due to the difficulties inherent in manufacturing shaped charges with entirely homogenous explosive fills [31], the possibilities of using liquid explosives within a shaped charge system have been assessed [32] [31] with positive results recorded. However, the majority of shaped charges in military service continue to use solid explosives as a main charge [20] [10] [4] as these compositions and their manufacturing processes are well understood.

3 Shaped Charge Modelling

Computer modelling is widely used for shaped charge research [14] [30] [16]. This is because computer modelling offers a safer, more cost effective and faster solution for energetics research than physical trials, with modern software offering a high degree of accuracy [33] [34].

This experiment will use the modelling software Abaqus [35] to compare the performance of two different shaped charge systems. While Abaqus is marketed for the modelling of structural integrity and vibration [35], the suite has been used for shaped charge research [36].

3.1 Shaped Charge Design Parameters

Due to the varied uses of shaped charges (outlined in Section 1.2), there is no single perfect shaped charge design and each system must be tailored to a specific purpose.

Shaped charge performance in the defence industry is generally measured by the depth of penetration of the jet into the target material [5] [20] [4], with military shaped charge systems designed to provide the greatest depth of penetration within certain design parameters.

This experiment will explore the influence of the material properties of the liner on the velocity of the jet produced. Two shaped charge systems will be modelled with identical geometry, and identical material properties for the explosive charge and the casing. The first system (System A) will be modelled with a copper liner, while the second system (System B) will be modelled with a titanium liner. In all other respects the systems will be identical.

3.2 Shaped Charge System Design

3.2.1 System Restrictions

It was decided that the shaped charge systems modelled would imitate those utlised within modern man-portable anti-tank systems. A common caliber for these is 84mm [10], therefore the system modelled was restricted to a diameter of 84 mm.

3.2.2 Liner Parameters

The optimal cone apex angle for a conical shaped change liner has been calculated to be between 40° and 60° [14]. Limitations of the Abaqus modelling software make a cone angle shallower than 50° problematic, and an angle of 50° was decided upon.

Allowing for 2 mm of casing thickness, the 50° cone angle resulted in a cone length of 90 mm, and a cone diameter of 80mm.

Research has indicated [5] [14] that the thickness of a shaped charge liner should be 4% of the cone diameter. This results in a cone thickness of 3.2 mm.

Parameter	Value
Cone angle	50°
Cone length	90 mm
Cone diameter	80 mm
Cone thickness	3.2 mm

Table 1 - Shaped charge liner dimensions

3.2.3 Casing Parameters

The limitation of 84 mm of overall system diameter and the 80 mm diameter of the liner informed a case wall thickness of 2 mm. As the explosive fill was to be initiated at a point along the base of the system, the thickness of the case in this area was increased to 6 mm.

A depth of explosive fill equal to half the charge diameter (40 mm) was placed at the base of the shaped charge liner, resulting in a total system length of 136 mm.

Parameter	Value (mm)
Case diameter	84
Case length	136
Case wall thickness	2
Case base thickness	6

Table 2 - Shaped charge system casing dimensions

3.2.4 Materials Used

The two systems modelled would be constructed of three separate sections; a casing, a liner and an explosive charge. The casing was modelled in stainless steel, this being a common choice for shaped charge casings [13] [37]. Stainless steel is a popular material for this role due to its ease of machining and low cost, as well as its compatibility with other materials. The explosive fill was modelled in TNT. TNT is well understood as a high explosive, and is therefore commonly used in computer modelling of blast effects [37] [30].

As copper is a popular material for shaped charge liners [13] [14] [3], it was decided that the liner for System A would be modelled in pure copper. Research into different liner materials [38] has indicated that Titanium has potential as a shaped charge liner due to its high ductility, low density and relatively high melting temperature [37]. The liner for System B was therefore modelled in pure Titanium.

Component	Material	
	System A	System B
Case	Stainless steel	
Explosive fill	TNT	
Liner	Copper	Titanium

Table 3 - Shaped charge system materials

4 2D shaped charge construction in Abaqus

4.1 Geometry

Initial sketches were made to create a 2D representation of a shaped charge with the dimensions laid out in section 3.2 above. These sketches were then extruded to create three parts: the shaped charge liner, the shaped charge casing and the HE fill.

The assembly module was then used to create the shaped charge system from these three parts.

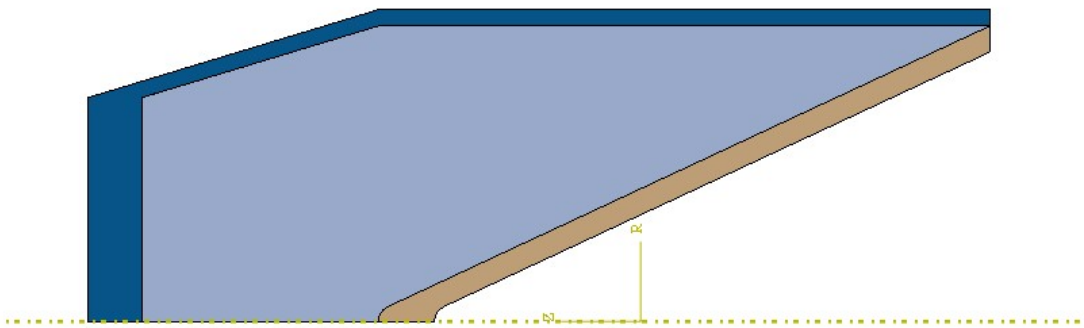

Figure 6 - 2D model of the shaped charge system

4.2 Materials and equations of state

The simulation used the Johnson-Cook constitutive model [39] for simulation of materials under high strain, strain rate and temperatures to model the effects of a high explosive shockwave on various metals, shown in Equation 1:

$$\sigma = (A + B\varepsilon^n)(1 + C \ln \dot{\varepsilon}^*)(1 - T^{*m})$$

Equation 1 - The Johnson-Cook model

Where:

- σ = stress
- A = initial yield stress
- B = strain hardening constant
- ε^n = equivalent plastic strain
- C = Strain rate hardening constant

- $\dot{\varepsilon}^{*}$ = normalised effective plastic strain rate
- m = thermal softening coefficient
- $T^{*} = \frac{T - T_{room}}{T' - T_{room}}$
- T_{room} = room temperature
- T' = melting temperature of the material

In addition to the Johnson-Cook model, the simulation also used the Jones, Wilkins & Lee model for the pressure, volume and energy behaviour of detonation products [40], shown in Equation 2:

$$P = A\left(1 - \frac{\omega}{R_1 v}\right)e^{-R_1 v} + B\left(1 - \frac{\omega}{R_2 V}\right)e^{-R_2 v} + \frac{\omega e_0}{v}$$

Equation 2 - The Jones, Wilkins & Lee model

Where:

- $v = \rho_e / \rho$ = relative volume between the detonation products and undetonated high explosive.
- P = pressure
- ρ_e = density of the explosive material
- ρ = density of the detonation products
- e_0 = specific internal energy
- A, B, and C = linear coefficients
- R_1, R_2, and ω = non-linear coefficients

The following materials were simulated in Abaqus:

Material	Role	Model Applied
Stainless steel	Casing	Johnson-Cook
Copper	Liner (System A)	Johnson-Cook
Titanium	Liner (System B)	Johnson-Cook
TNT	Explosive charge	Jones, Wilkins & Lee

Table 4 - Materials and equations of state used (2D model)

Using the following material properties [41] [42]:

Material	A (MPa)	B (MPa)	n	M	C	ρ (kgm^{-3})	E (GPa)	v	$\theta_{transition}$	θ_{melt}
Steel	350	275	0.36	1.00	0.022	8960	125	0.34	293K	1811K
Copper	90	292	0.31	1.09	0.025	7850	210	0.3	293K	1790K
Titanium	1030	1680	0.69	1.40	0.018	4314	123	0.33	293K	1935K

Table 5 - Johnson-Cook properties used

And the following properties for the explosive fill [37]:

Material	ρ (g/cm^3)	Velocity of detonation (ms^{-1})	A (GPa)	B (GPa)	R1 n/a	R2 n/a	ω n/a	Pre-detonation bulk modulus (GPa)	Detonation energy Density (Jkg^{-1})
TNT	1.717	7980	524.23	7.68	4.2	1.1	0.34	9.00	3680000

Table 6 - Jones, Wilkins & Lee properties used

The properties above were entered into Abaqus and a section for each was created, as shown below.

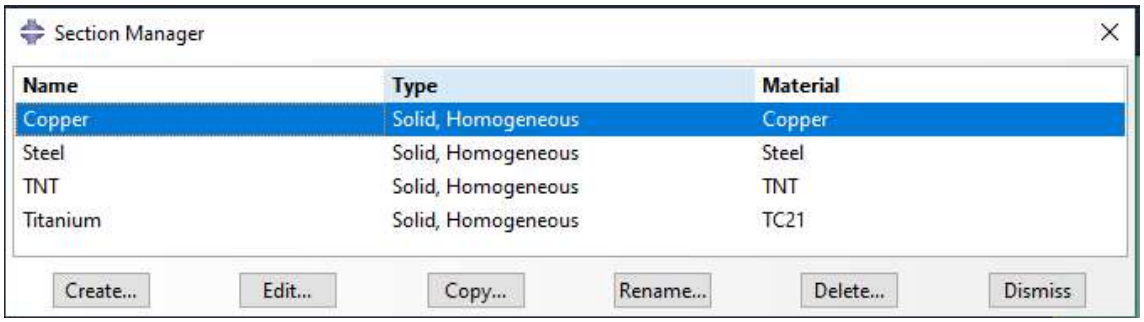

Figure 7 - Material sections created in Abaqus

4.3 Boundary conditions and detonation point

In order to simulate a symmetrical and enclosed shaped charge system, boundary conditions were set on the interior edge of the liner, HE fill and case. This would restrict these components from movement in the negative X direction.

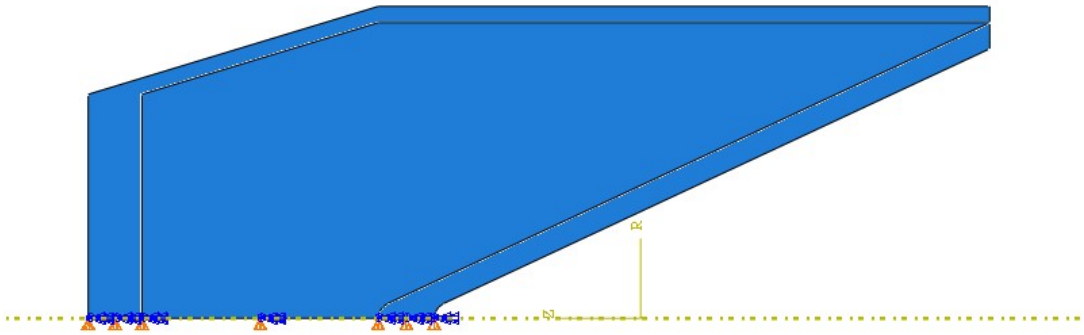

Figure 8 - 2D model of the shaped charge system with boundary conditions shown on the lower edge

A detonation point for the HE fill was chosen at the base of the charge in what would, in a symmetrical shaped charge assembly, be the centre of the charge diameter. This detonation point would 'initiate' the HE fill at t=0 of the simulation.

4.4 Meshing

During the initial meshing of the 2D design, it was anticipated that the Abaqus simulation would fail due to excessive deformation as elements were stretched beyond the limits which the software could process.

To investigate which elements would deform first, the initial mesh created showed a uniform mesh size throughout the design. The simulation was run, and the results showed that a single element at the base of the liner had deformed excessively when accelerated by the explosive shockwave, causing the simulation to fail.

In an attempt to resolve this, the liner meshing was reconfigured to produce a graduated mesh which was wider at the top of the liner, gradually decreasing in size to show smaller elements at the base of the liner. It was expected that this

mesh size would allow more fluid movement of the elements and reduce the excessive deformation.

As the mesh size was decreased at the base of the liner, it was also necessary to reduce the size of the mesh for the explosive composition directly behind the liner to ensure a smooth transition between the two. The explosive charge was therefore re-meshed using a graduated mesh along the central axis, beginning with a larger mesh size at the base of the charge and moving to a finer mesh where the charge met the base of the liner.

When the simulation was run with the adjusted mesh, excessive element distortion continued to occur, however the simulation was able to run for long enough to gather the required data.

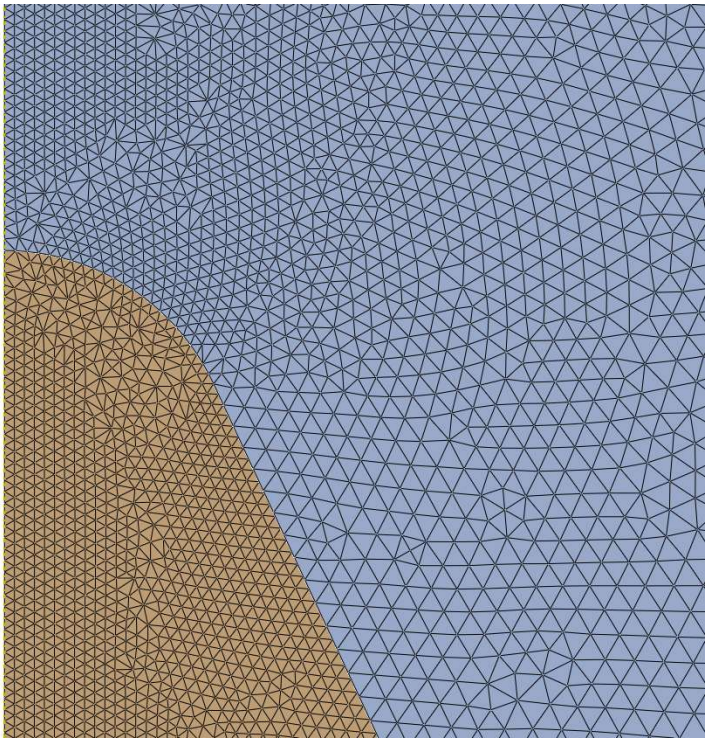

Figure 9 - Detail of the mesh for the 2D model, showing the section where the explosive fill meets the base of the liner

Figure 10 - Screenshot showing the distorted elements in early simulations (highlighted in red)

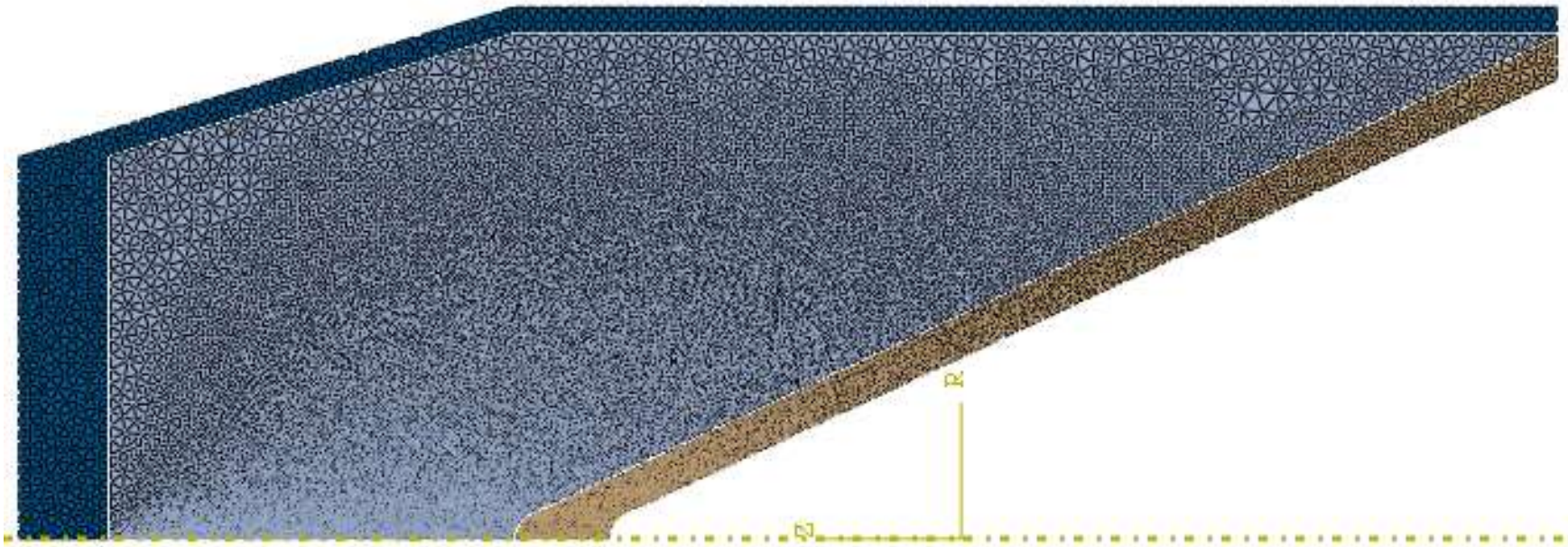

Figure 11 - The final mesh for the 2D model

5 3D shaped charge construction in Abaqus

5.1 Geometry

The 3D design was created from the same sketches as the earlier 2D designs, with the parts created as 3D revolutions as opposed to 2D extrusions, creating the model shown below:

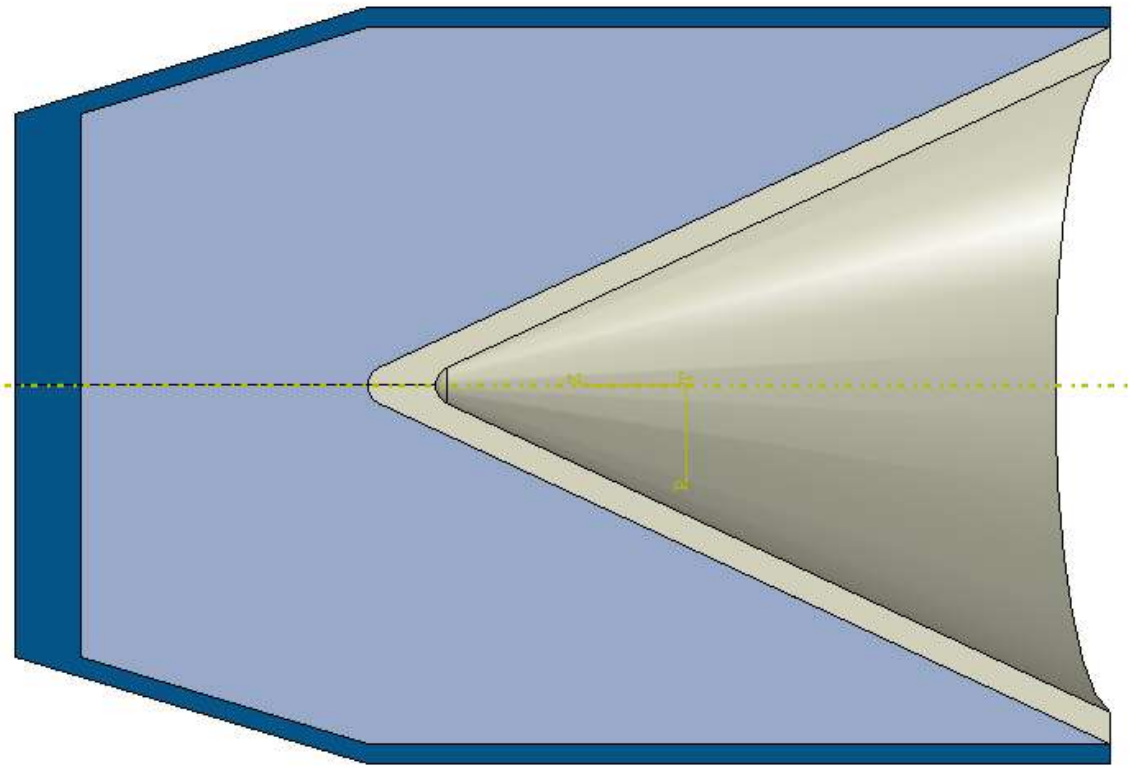

Figure 12 – Initial 3D model of the shaped charge system

The elements were revolved to 180° to create a hemispherical model of the shaped charge system. This was to facilitate the meshing of areas such as the base of the liner, which would be difficult to access in a full 360° revolution.

5.2 Boundary conditions and detonation point

As in the 2D simulation, boundary conditions were applied to the 3D model to simulate the presence of a second half of the shaped charge system:

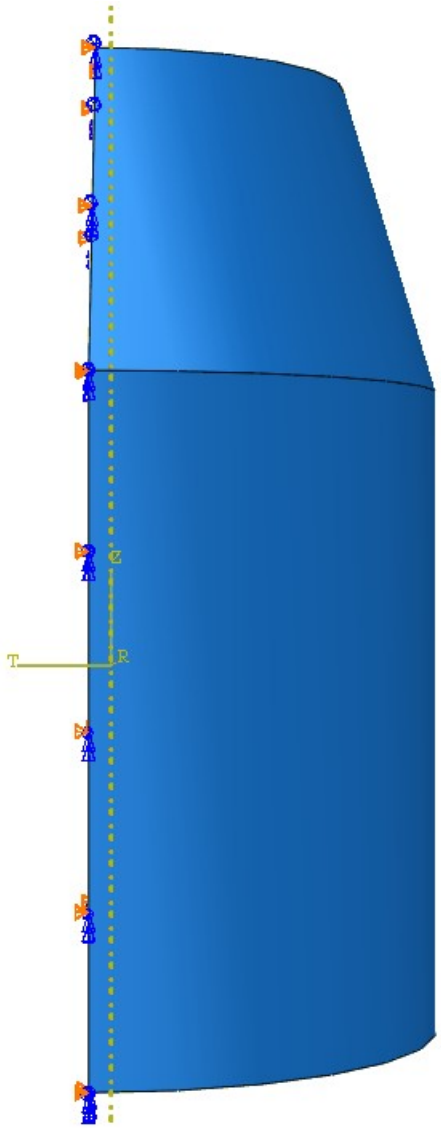

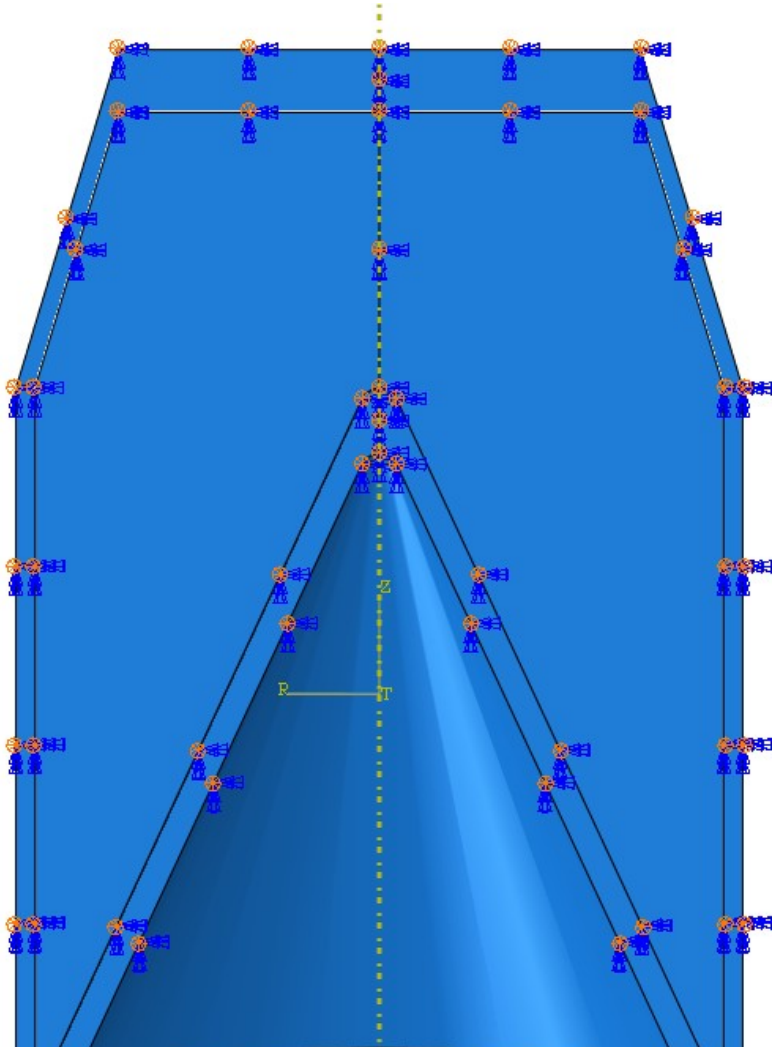

Figure 13 - Boundary conditions applied to the 3D model

5.3 Materials and equations of state

As the 3D model was based heavily on the previous 2D model, the same equations of state and material properties were used to replicate System A in 3D:

Material	Role	Model Applied
Stainless steel	Casing	Johnson-Cook
Copper	Liner	Johnson-Cook
TNT	Explosive charge	Jones, Wilkins & Lee

Figure 14 - Materials and equations of state used (3D model)

5.4 Meshing

The 3D design presented new challenges during the meshing phase due to the element limit within the Abaqus software, which prevents a simulation being run on a model containing greater than 250,000 elements.

In order to 'budget' these elements for as finer mesh in the base of the liner and associated areas of the HE fill, a coarse mesh was used for the shaped charge casing. This mesh was significantly coarser than the mesh used for even the outer areas of the HE fill, however the results of the 2D simulations had shown that the case was readily deformed by the pressures created by the expanding HE, with no simulations crashing due to element collisions in this area.

As with the 2D simulations, a relatively coarse and even mesh was created in the liner and HE fill to discover if element deformation in 3D would occur in similar areas to the 2D simulations. This was initially the case, and the base of the liner and the areas of HE interfacing with this were remeshed to describe a graduated mesh, with finer elements at the very base of the liner, slowly increasing in size throughout the distance from the liner base to the tip. A simulations was run with this mesh, which ran for long enough to provide meaningful results.

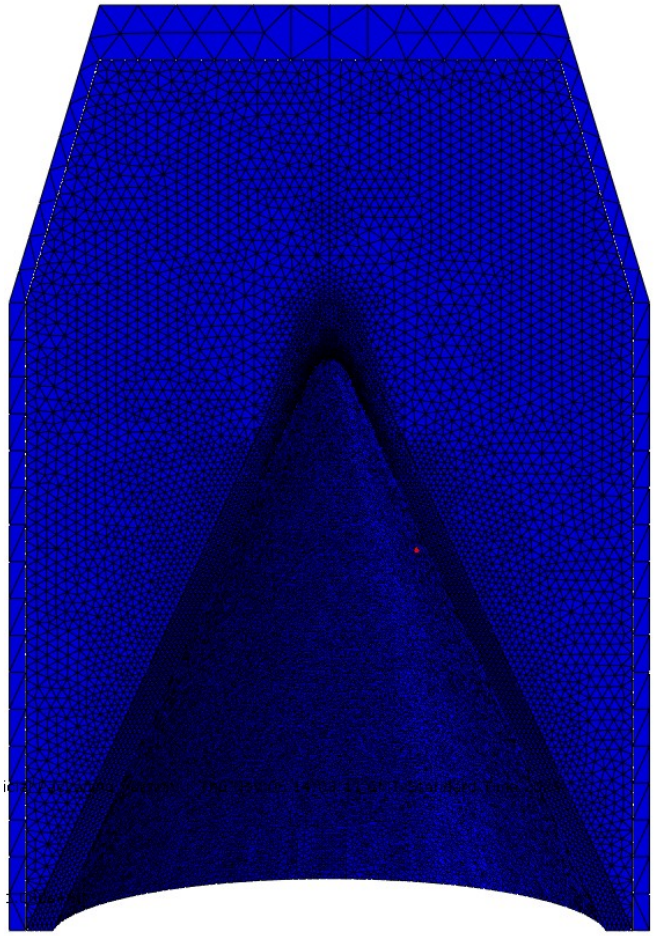

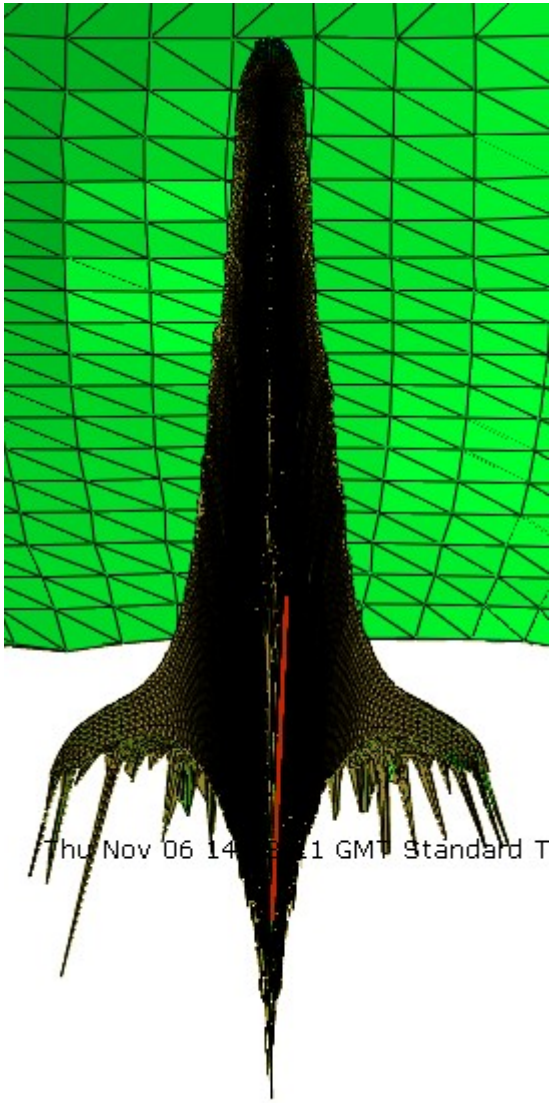

Figure 15 - Elements excessively deformed during the 3D simulation (highlighted in red)

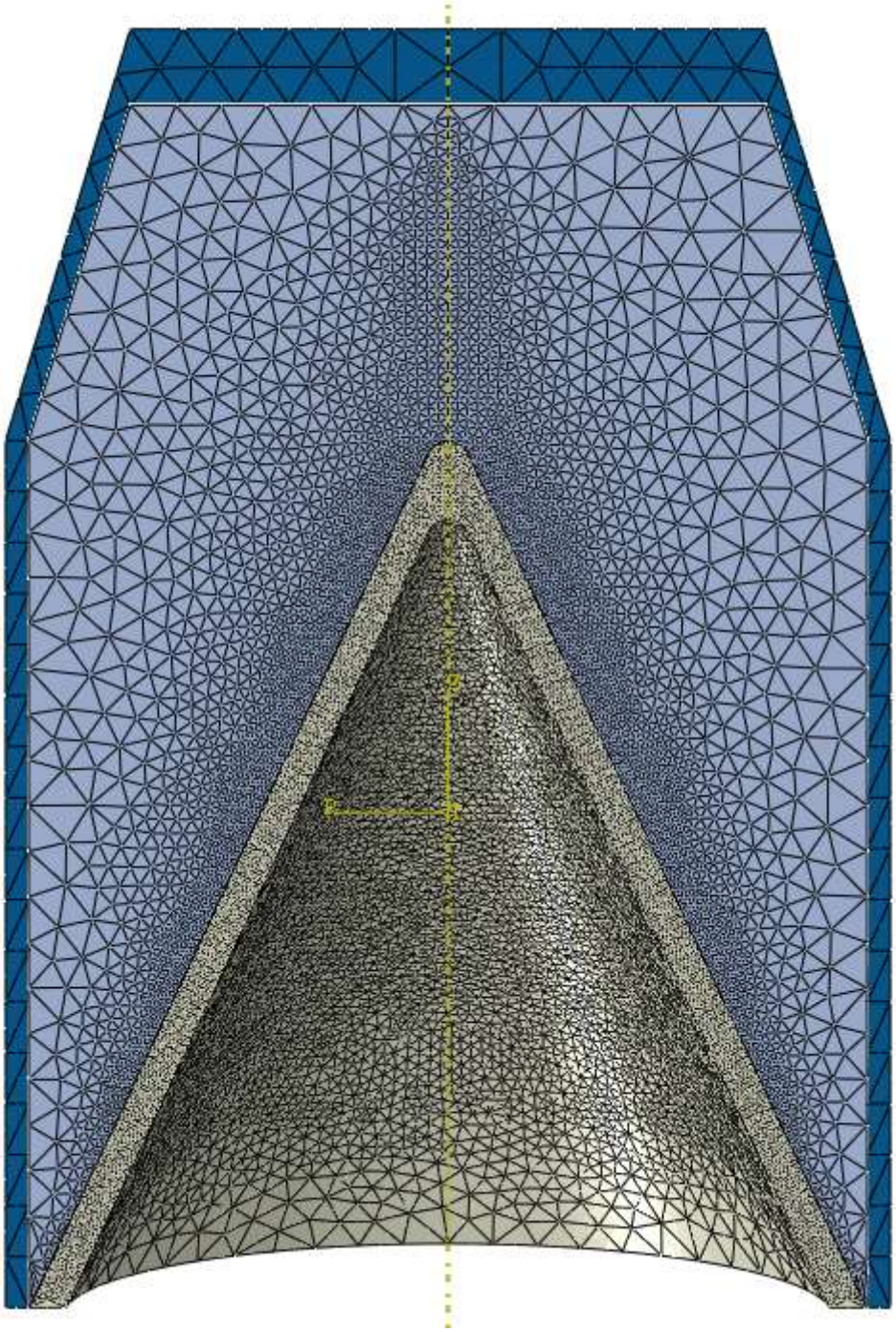

Figure 16 - The final mesh for the 3D model

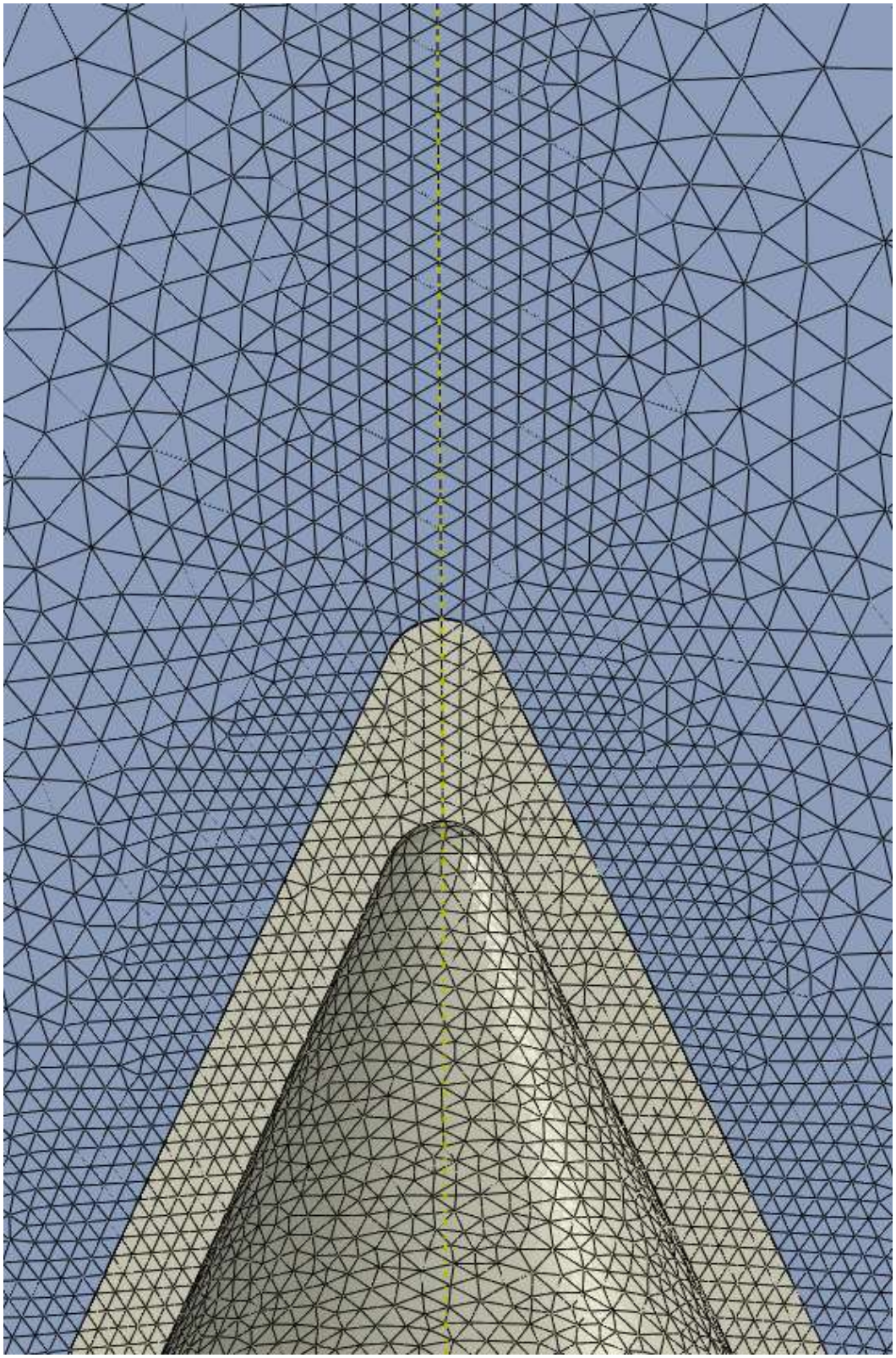

Figure 17 - Detail of the mesh graduation, showing the matching of element sizes along the charge/liner border

5.5 Dynamic remeshing and smooth particle hydrodynamics

The two 2D simulations and the successful 3D simulation provided sufficient results for analysis, however with lab time remaining it was decided that the use of the Arbitrary Lagrangian Eularian (ALE) dynamic remeshing and Smooth Particle Hydrodynamics (SPH) features of the Abaqus software could potentially enable simulations to run for longer before crashing.

Simulations using ALE or SPH are far more computationally expensive than the ‘standard’ simulations which had been used up to this point. In order to streamline the simulations as much as possible, both the shaped charge liner and HE fill were partitioned so that ALE or SPH could be applied only to smaller areas where excessive element deformation had historically been a problem.

To create partitions, the sketches for the liner and HE fill were revisited. The trim tool was used to cut sections out of these sketches, converting each from a single part sketch to two separate parts, a larger area where standard simulation settings would be applied, and a smaller area where ALE or SPH could be applied. These two parts, such as the tip of the liner and the remaining liner area, were then joined together in the Assembly stage of the simulation to create a composite part.

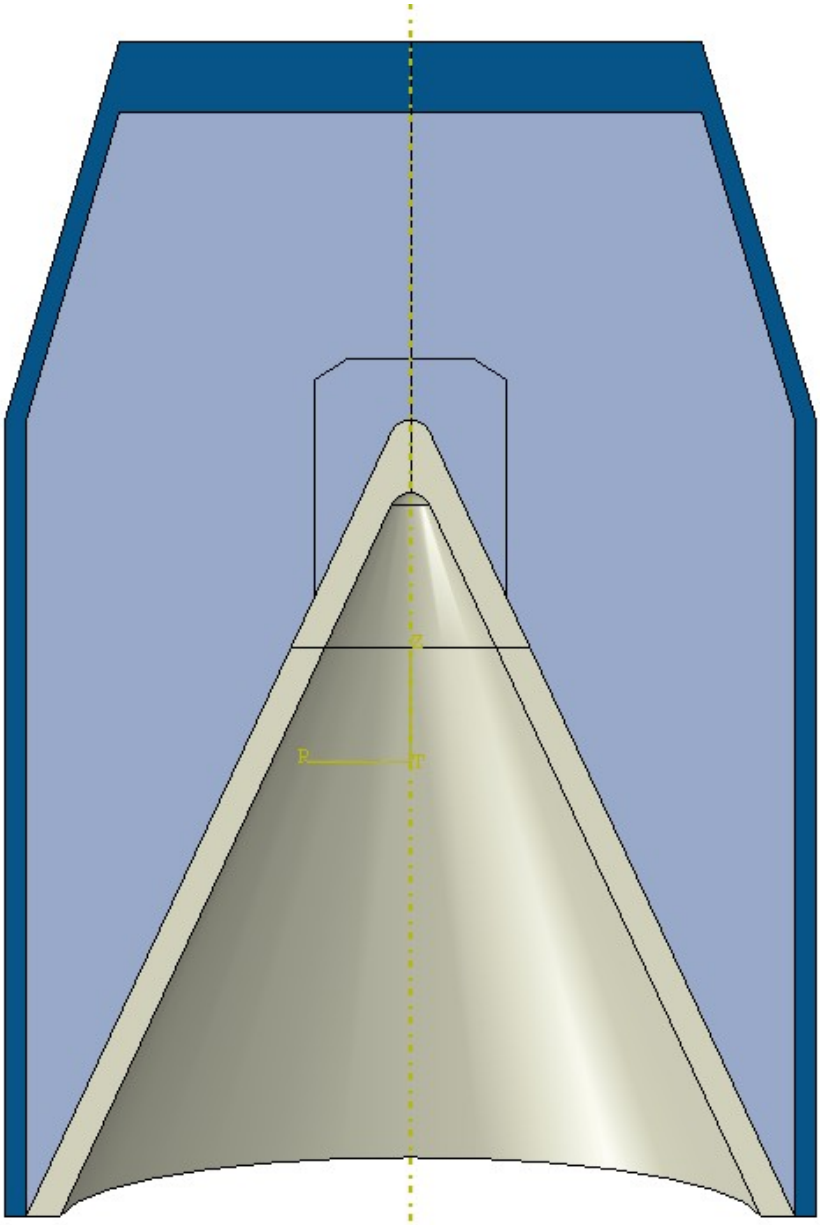

Figure 18 - The 3D model used in SPH and ALE simulations, showing the smaller sections created

5.5.1 Dynamic remeshing

The ALE dynamic remeshing feature in Abaqus is a feature which enables excessively deformed elements to be ‘re-meshed’ while the simulation is running, theoretically removing the issue of excessively deformed elements crashing the simulation, which had been a feature of the investigations described in this report.

ALE was applied to the liner using the settings shown below:

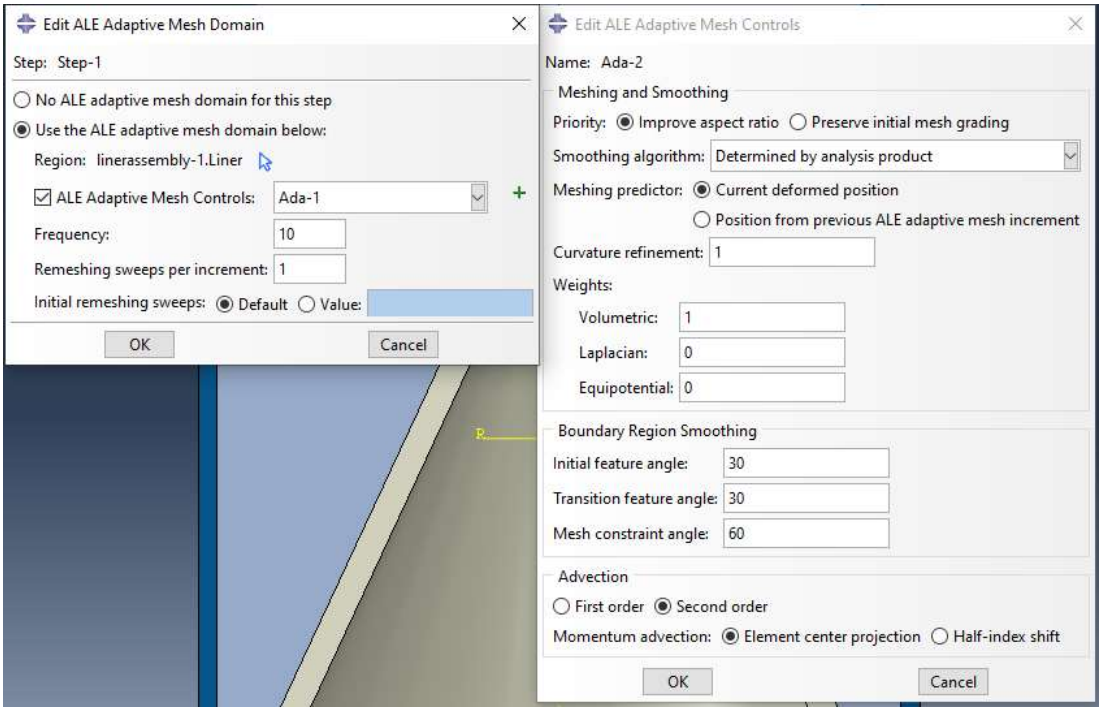

Figure 19 - ALE settings used for the 3D simulation

Surfaces were then assigned to the outer surface of the liner and the inner surface of the charge in direct contact with the liner. An interaction was created between these two surfaces:

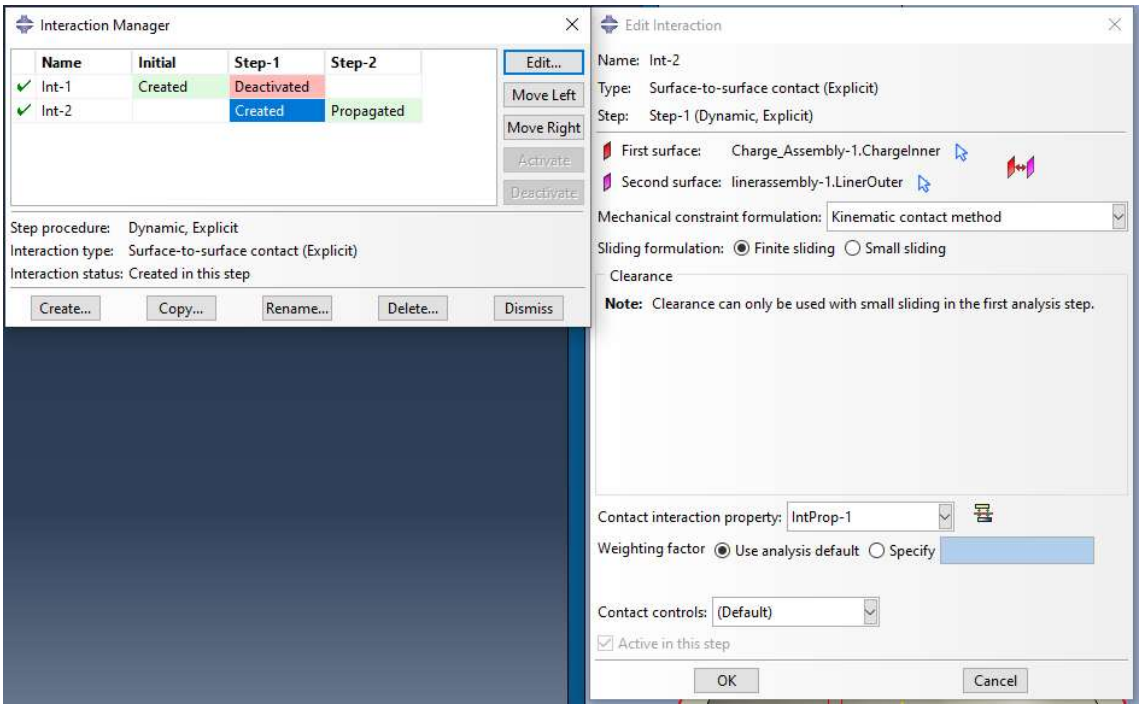

Figure 20 - ALE surface interactions

5.5.2 Smooth particle hydrodynamics

While Dynamic Remeshing is concerned with the translation of excessively deformed elements into multiple undeformed elements, another potential cure solution for this issue is the use of SPH. SPH deals with the problem of excessively deformed elements by converting these deformed elements into particles which, theoretically, will be free to remove themselves from the assembly, allowing the simulation to run for longer.

SPH was enabled within the Mesh module in Abaqus, as shown below:

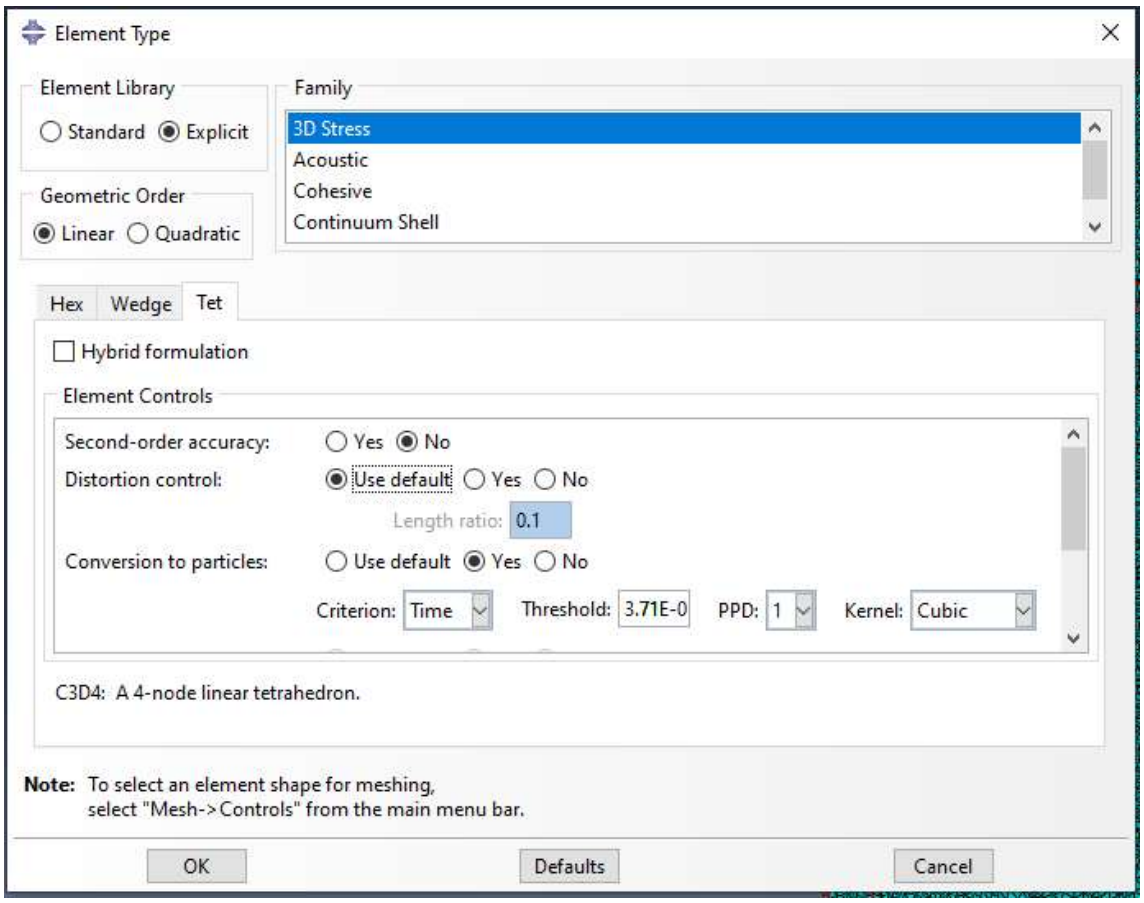

Figure 21 - SPH settings used for 3D simulation

6 Results

6.1 System A (copper liner)

6.1.1 Velocity

The velocity of five nodes at the base of the shaped charge liner was tracked through the simulation.

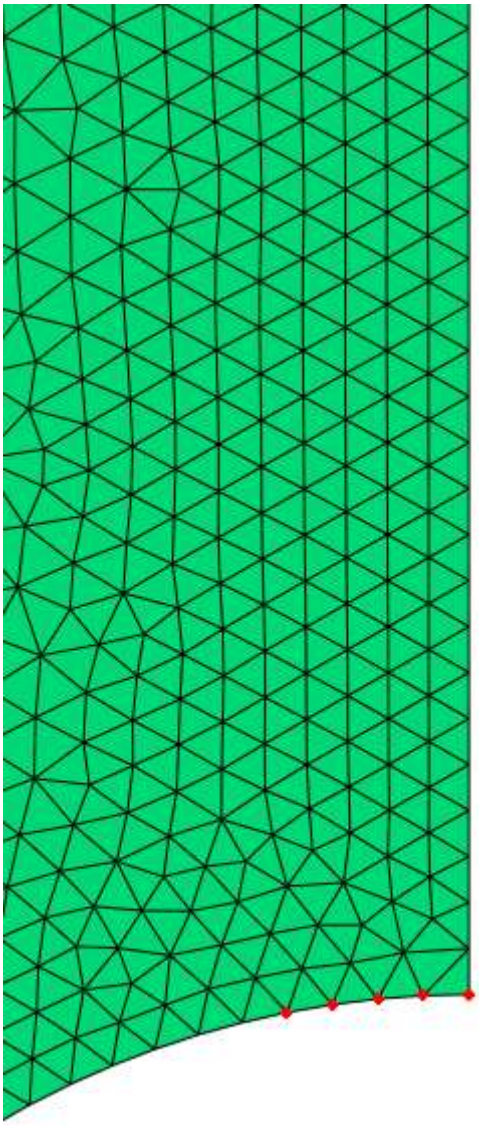

Figure 22 - Nodes selected at the base of the copper liner

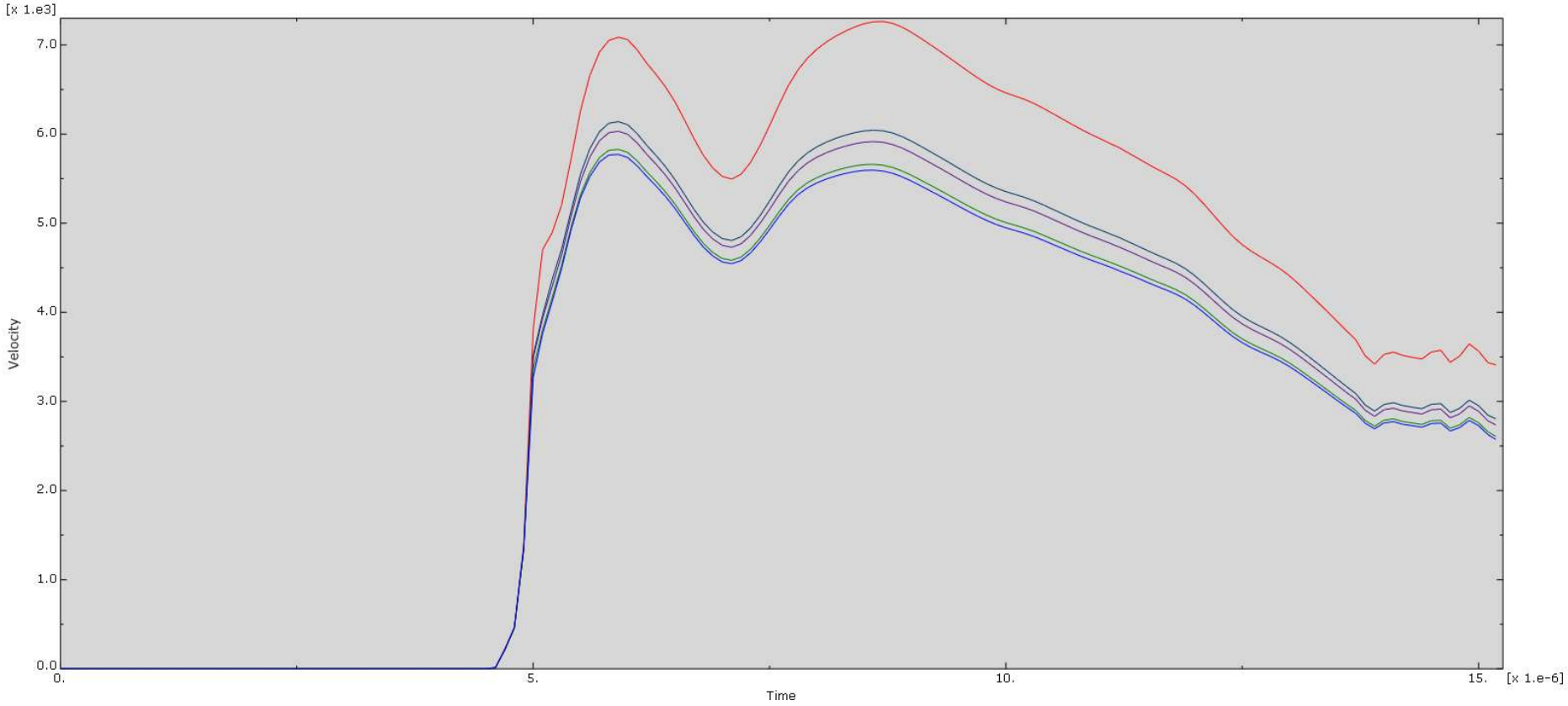

Graph 1 - Velocity of liner nodes (System A)

Graph 1 shows the rapid acceleration of the selected nodes at t=~5E-06 s, the point in time where the shockwave generated by the high explosive detonation reaches them. The acceleration is almost instantaneous to a velocity of roughly 3.5E3 m/s, and then increases more gradually to the region of 6E3 m/s. The velocity then begins to decline steadily.

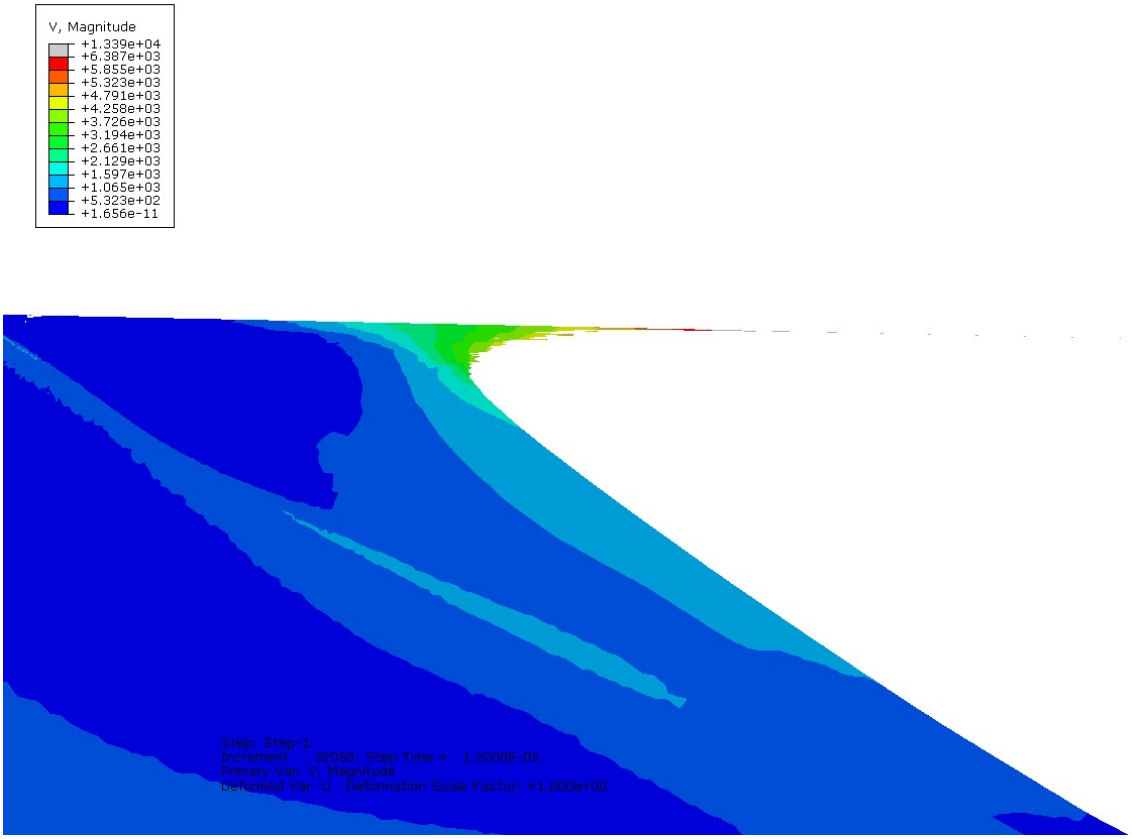

Figure 23 - Velocity of the shaped charge liner (System A)

Figure 25 illustrates the acceleration of the nodes at the base of the shaped charge liner approvimately 2 ms after the shockwave reaches it. The nodes accelerated by the shockwave can be clearly seen in red.

6.1.2 Pressure

The following screenshots show the pressure wave as it passes through the system, from the ignition point within the high explosive to the end of the casing.

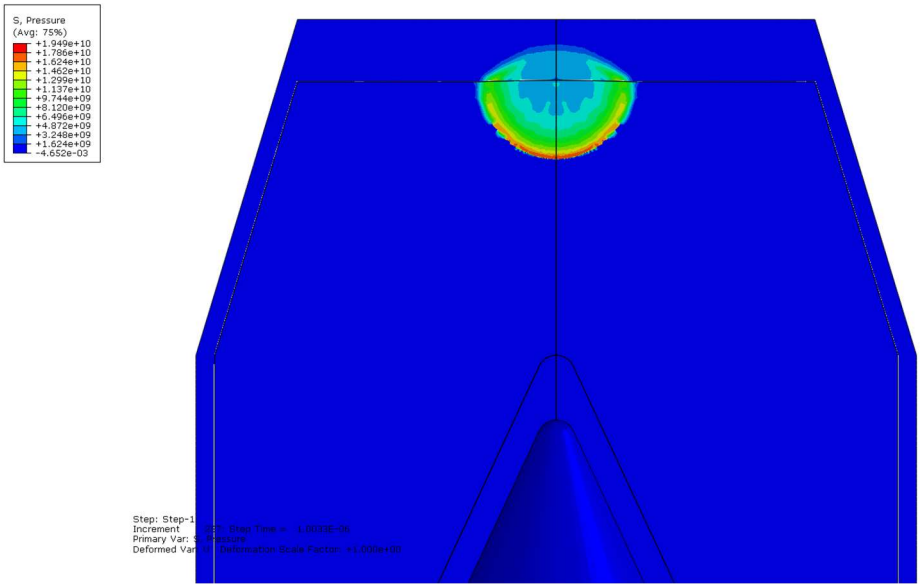

Figure 24 – Pressure wave within System A (t=1.0033E-06 s)

Figure 26 shows a hemispherical pressure wave moving outwards from the detonation point at the base of the high explosive charge. The highest pressures are observed on the leading edge of the detonation wave, and the wave can be seen propogating more rapidly through the explosive fill than through the steel casing.

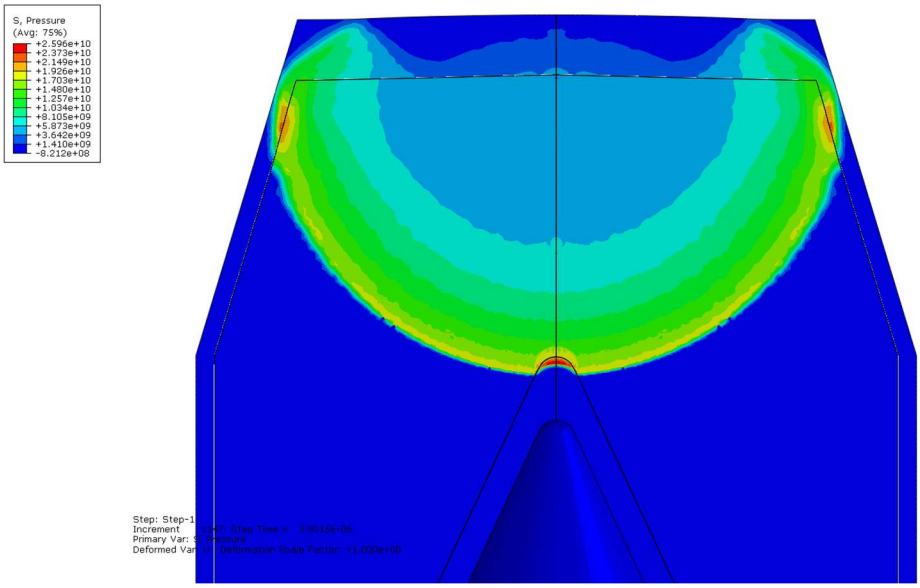

Figure 25 - Pressure wave within System A (t=3.8015E-06 s)

Figure 27 shows the pressure wave created by the explosive detonation as it interacts with the shaped charge liner. Due to the change in material density as the wave passes from the TNT fill to the copper liner, a significant increase in pressure is observed at the base of the liner.

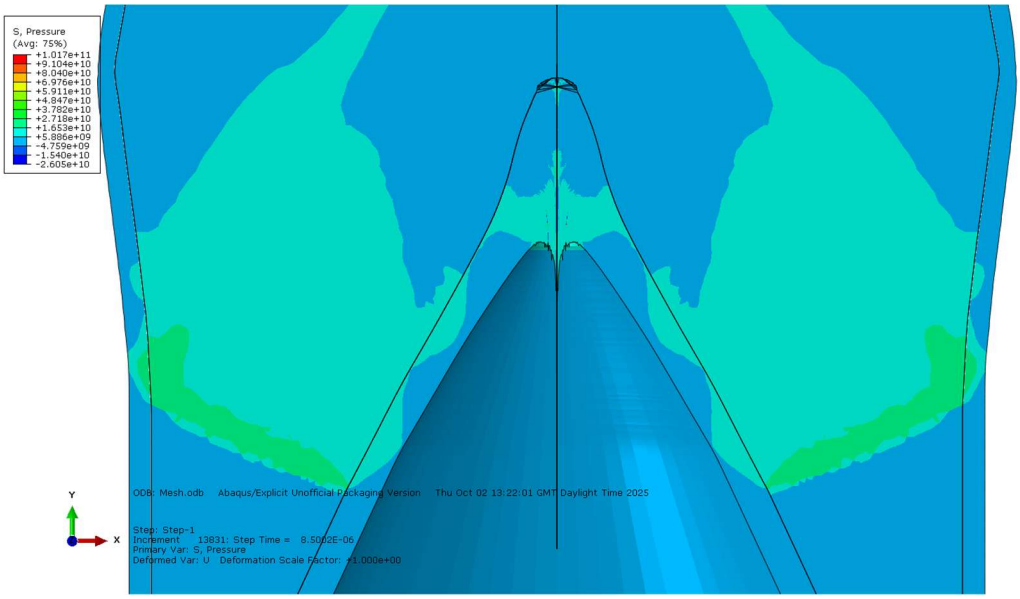

Figure 26 - Pressure wave within System A (t=8.5E-06 s)

Figure 28 shows the bifurcation of the pressure wave as the explosive shockwave moves up each side of the shaped charge liner. This results in a symmetrical pressure wave moving up the outside of the liner.

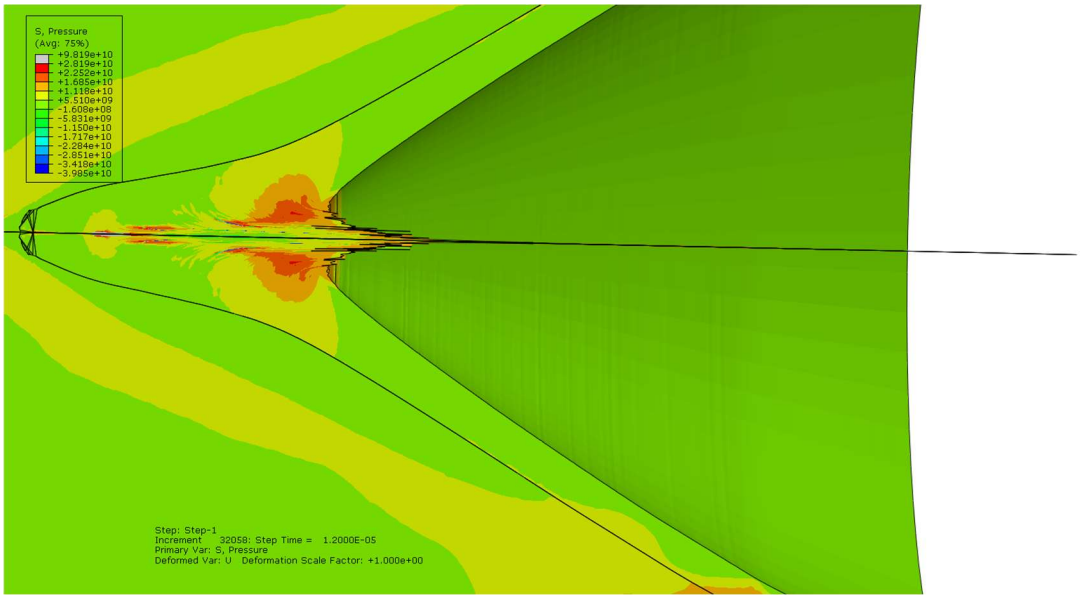

Figure 27 - Pressure wave within System A (t=1.2E-06 s)

Figure 29 shows the pressures created within the shaped charge liner by the pressure wave seen in figure 28. Areas of extreme high pressure are observed at the centre of the liner, resulting in the formation of a copper jet.

6.1.3 Maximum principal stress

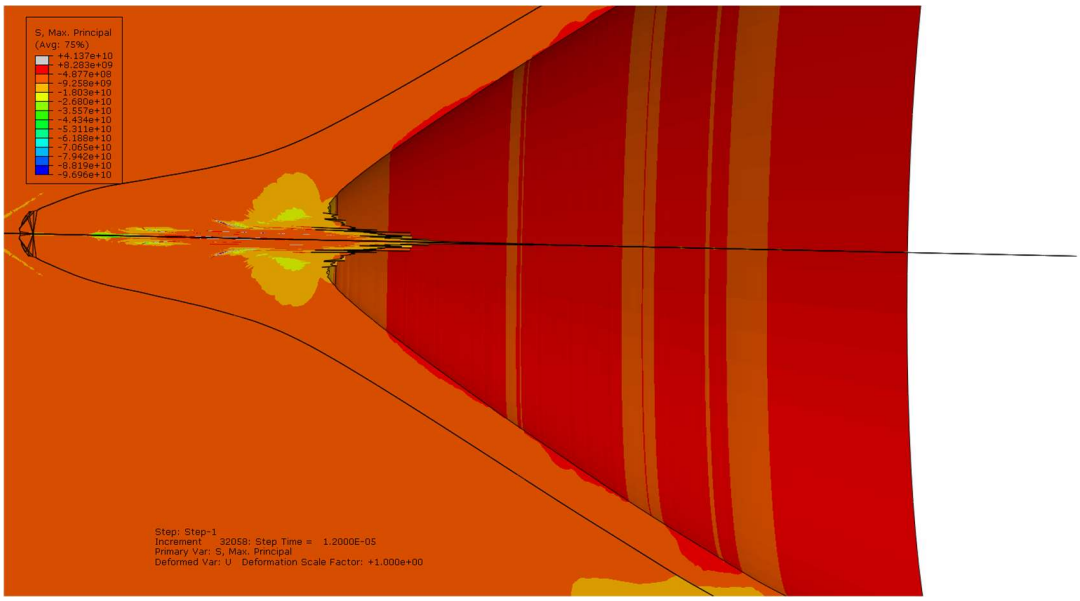

Figure 28 - Max principal stress within System A (t=1.2E-05 s)

Figure 30 illustrates the relationship between the pressure wave and the stresses created within the shaped charge liner. Rings of alternating tension (red) and

compression (orange) can be seen where the explosive shockwave is acting upon the copper liner, with areas of extreme compression (yellow) observed at the base of the liner.

6.2 System B

6.2.1 Velocity

The velocity of five nodes at the base of the shaped charge liner was tracked through the simulation. These nodes were in the same position as those tracked during the simulation of System A.

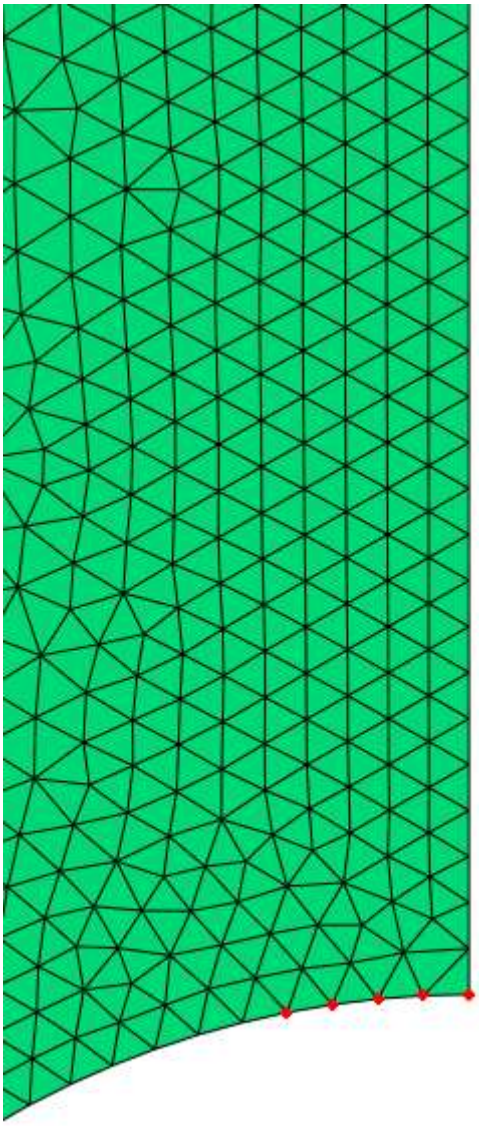

Figure 29 - Nodes selected at the base of the titanium liner

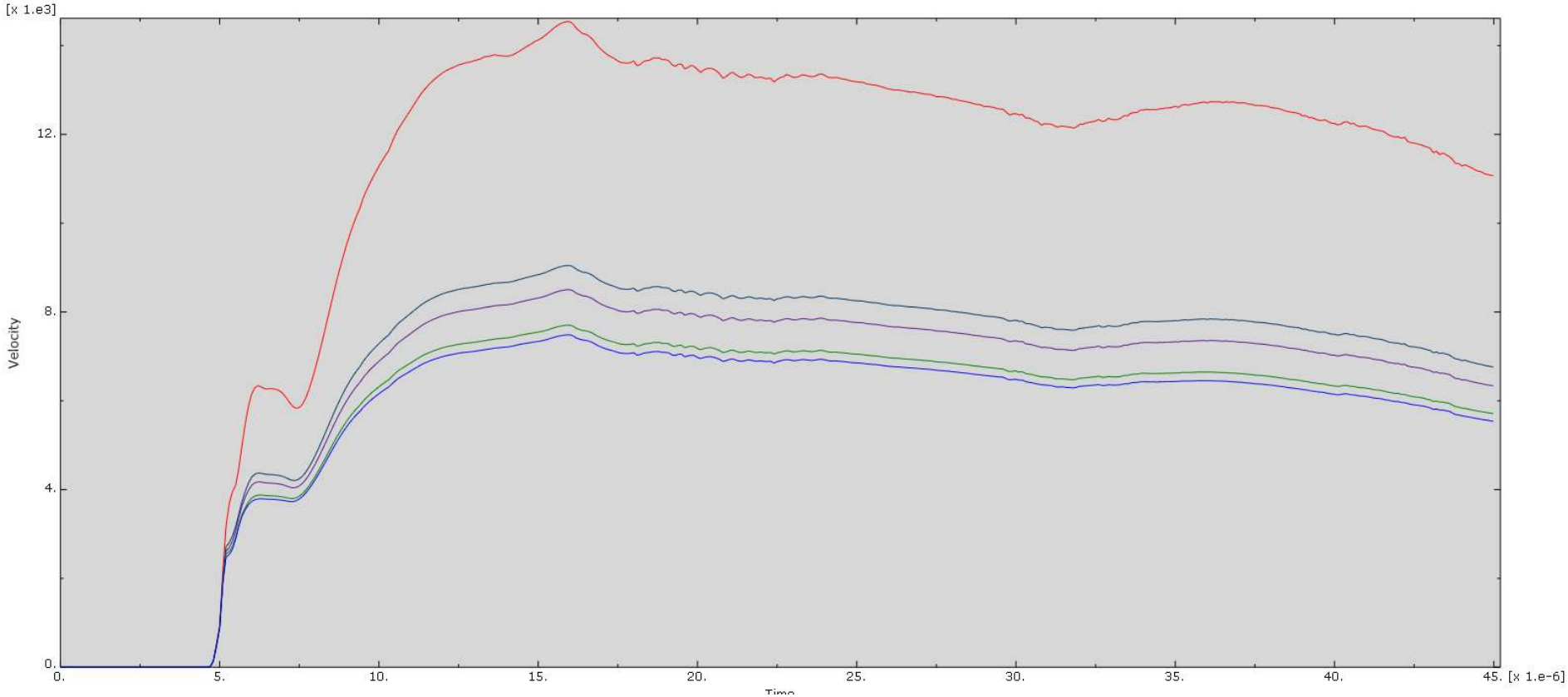

Graph 2 - Velocity of liner nodes (System B)

Graph 2 shows the rapid acceleration of the selected nodes at t=~5E-06 s, the point in time where the shockwave generated by the high explosive detonation reaches them. The acceleration is almost instantaneous to a velocity of roughly 4E3 m/s, and then increases more gradually, but still rapidly, to the region of 8E3 m/s. The velocity then begins to decline steadily.

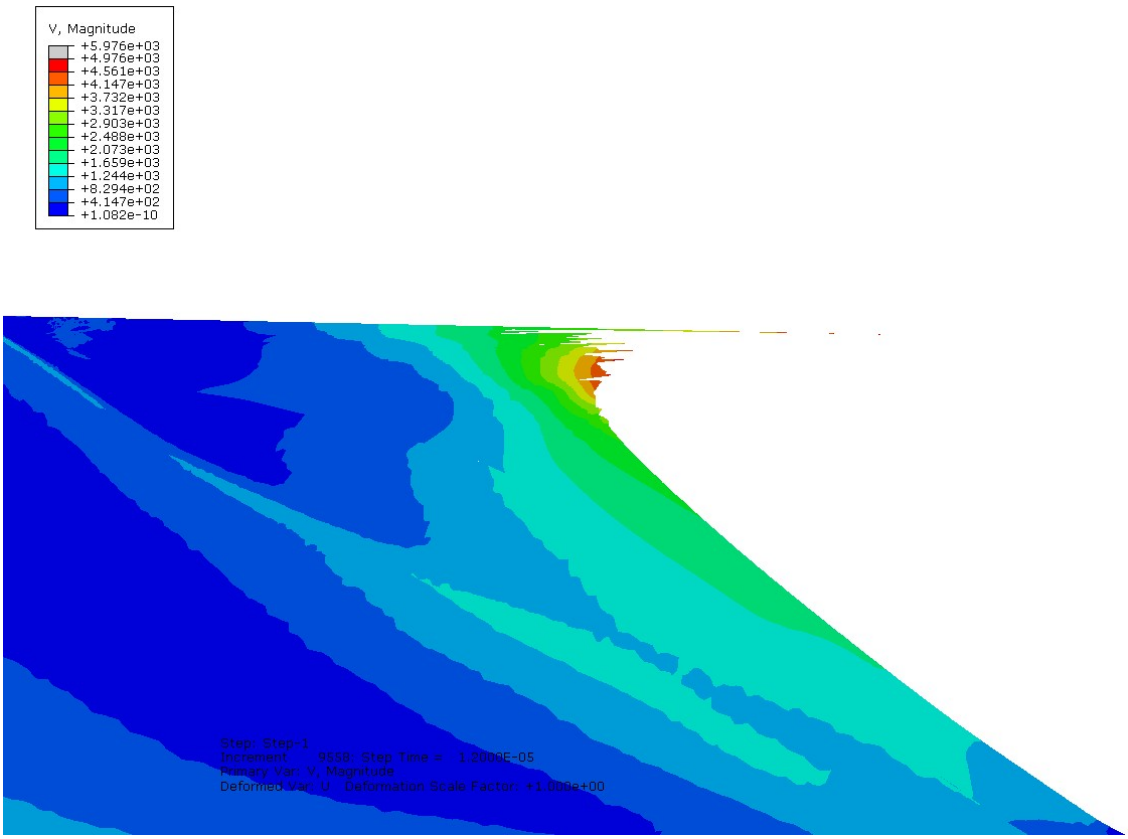

Figure 30 - Velocity of the shaped charge liner (System B)

Figure 32 illustrates the acceleration of the nodes at the base of the shaped charge liner approvimately 2 ms after the shockwave reaches it. The nodes accelerated by the shockwave can be clearly seen in red.

6.2.2 Pressure and stress

As the explosive fill for System B was identical to that of System A, the pressures observed during the System B simulation were comparable to those observed with System A, with high pressures created at the base of the shaped charge liner on contact with the explosive shockwave.

6.3 3D simulation

6.3.1 Velocity

As with the 2D simulations, five nodes at the base of the shaped charge liner were selected for velocity tracking. These are shown in red below.

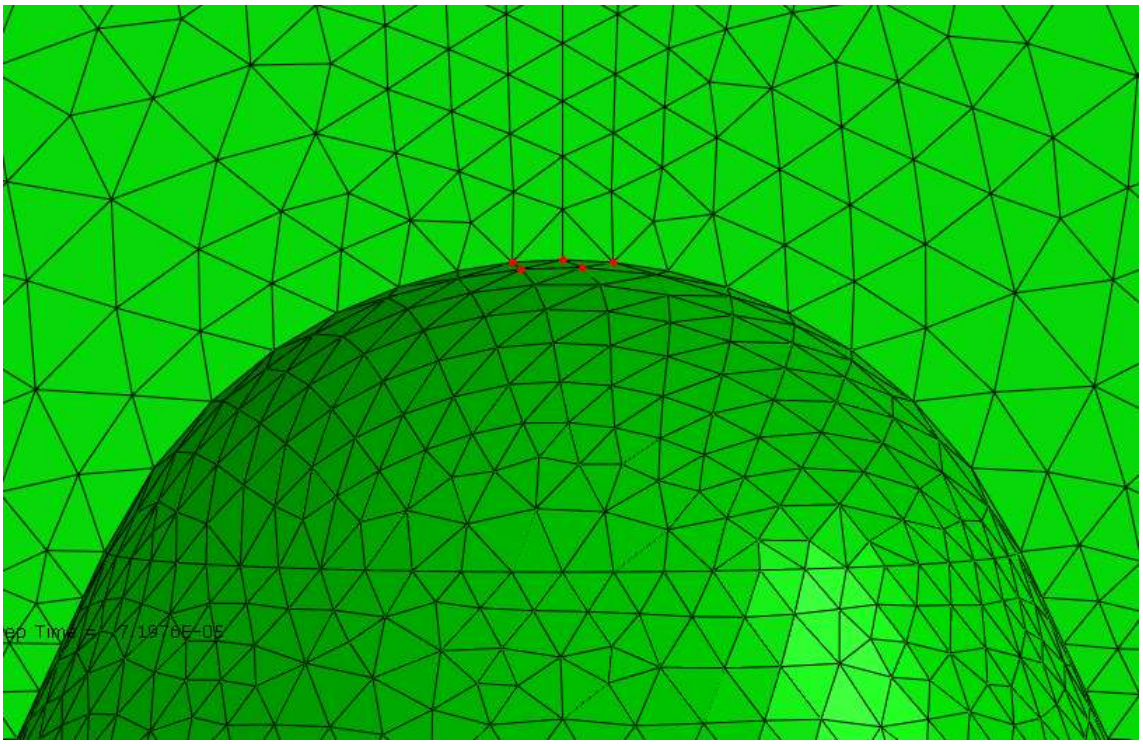

Figure 31 - Nodes selected at the base of the 3D liner

The velocity of the nodes selected is shown in Graph 3, below:

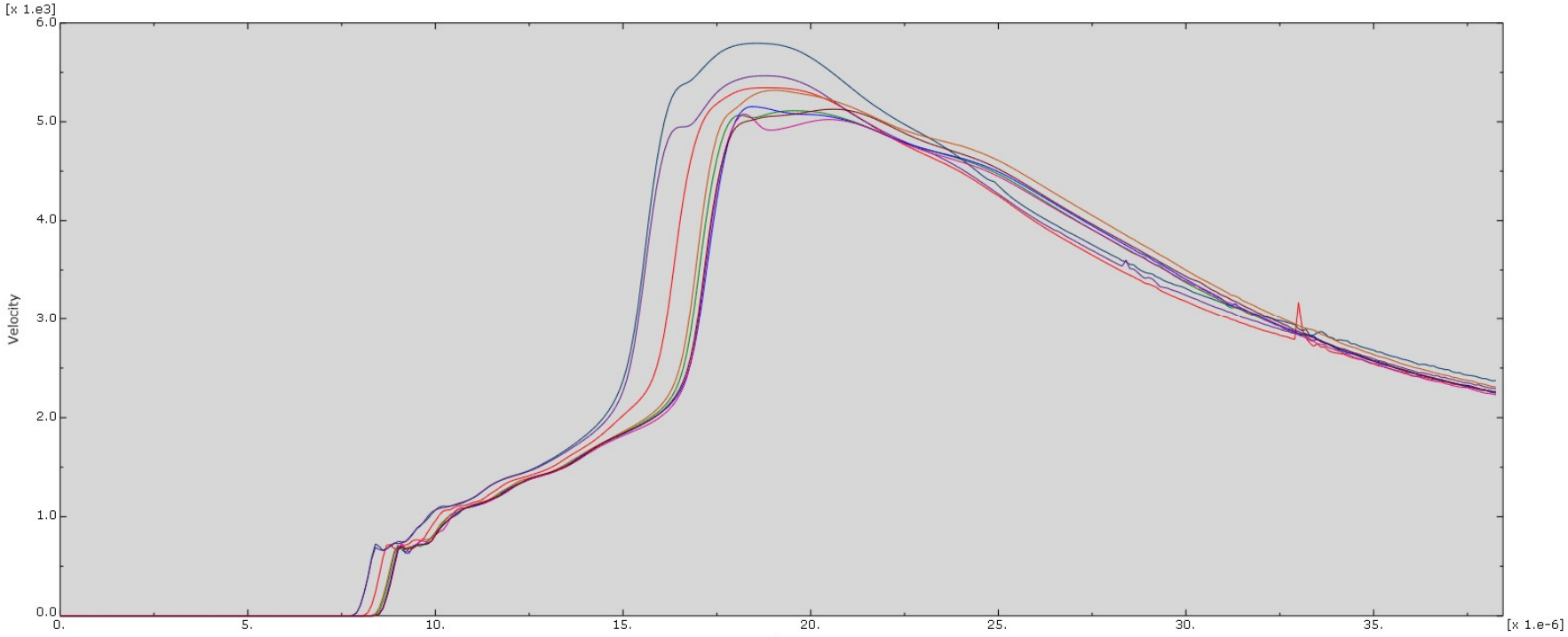

Graph 3 - Velocity of liner nodes (3D)

Graph 3 shows an initial rapid acceleration to 1E3 m/s at roughly t=7E-06 s, with a more gradual increase to 2E3 m/s, followed by a second rapid acceleration to 5E3 m/s at roughly t=15E-06 s.

A gradual deceleration is then observed, with velocity falling back to the region of 3E3 m/s when the simulation ends.

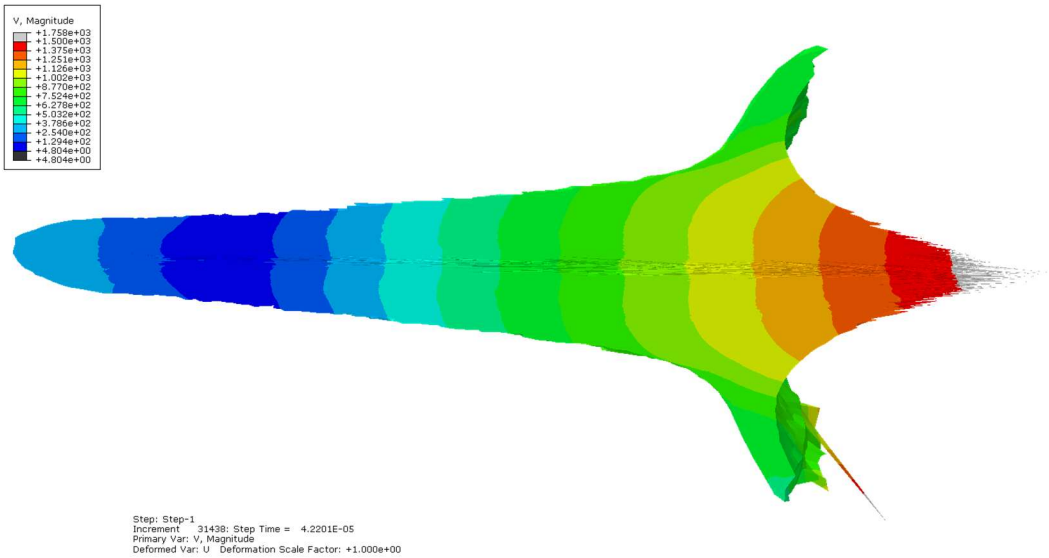

Figure 32 - Velocity of the shaped charge liner (3D)

Figure 34 illustrates the velocity of the shaped charge liner at t=4.22E-05 s, at the end of the simulation. This shows a clear graduation in the node velocities throughout the liner, with the highest velocities (1.73E3 m/s, shown in grey) at the front and lower velocities (4.8 m/s, shown in dark blue) at the rear.

6.4 3D simulation (SPH)

6.4.1 Velocity

After enabling SPH in the 3D simulation, a number of liner nodes were selected and their velocity tracked. Graph 4 shows a similar velocity profile to that seen in Graph 3, due to the identical materials and parameters used in both simulations.

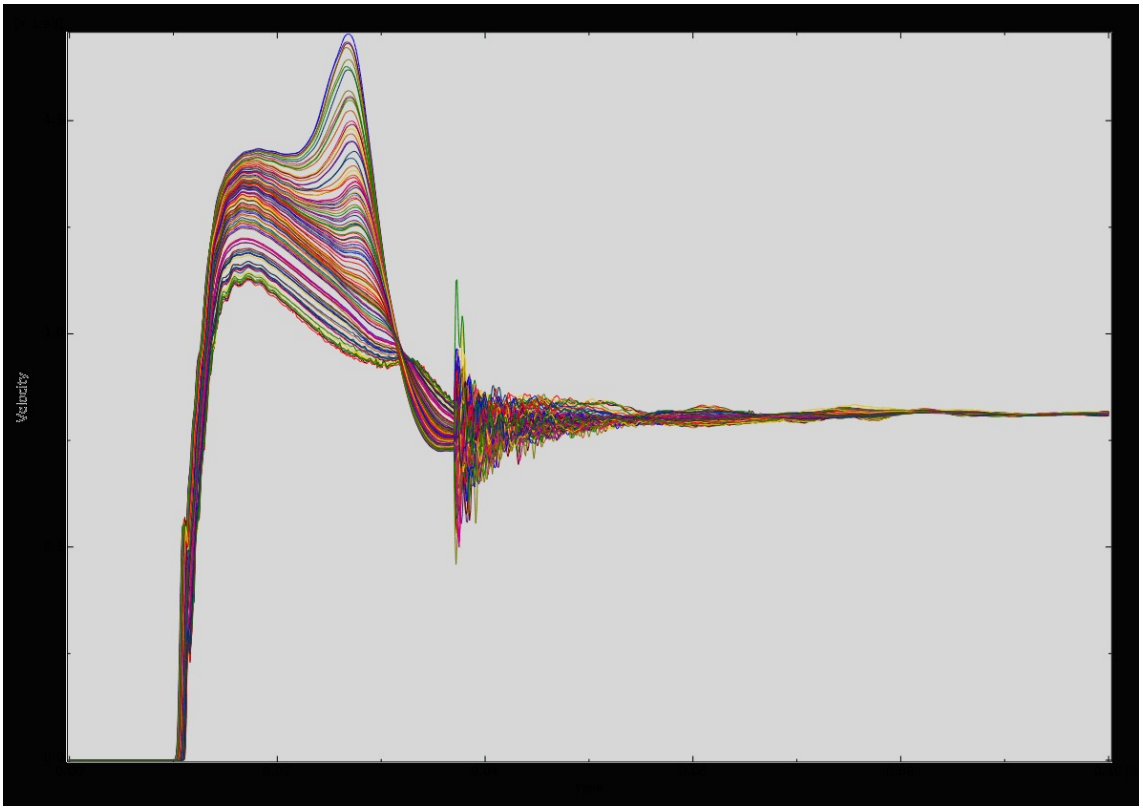

Graph 4 – Velocity of liner nodes (3D, SHP enabled)

Graph 4 shows a sudden increase in velocity of the selected nodes, followed by a brief period of stability before a second, slower increase. The velocity then drops rapidly to about 50% of peak, before levelling out.

7 Discussion

7.1.1 Velocity (System A and System B)

Graphs 5 and 6 show the differences in reaction of the copper and titanium liners to the shockwave produced by the detonation of the high explosive fill.

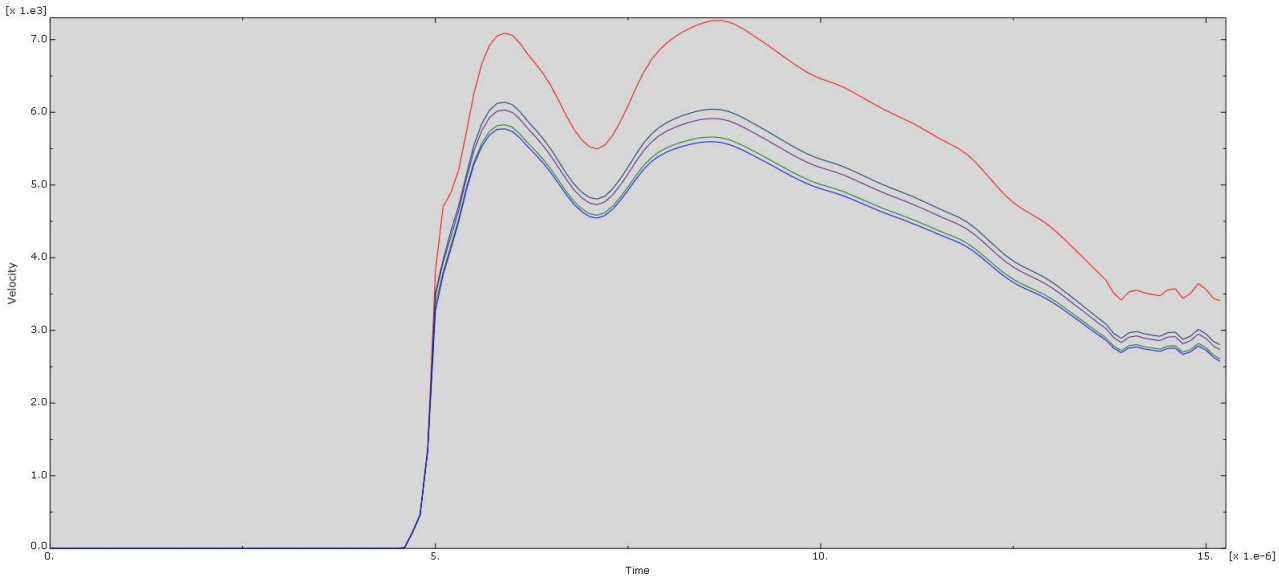

Graph 5 - Copper liner

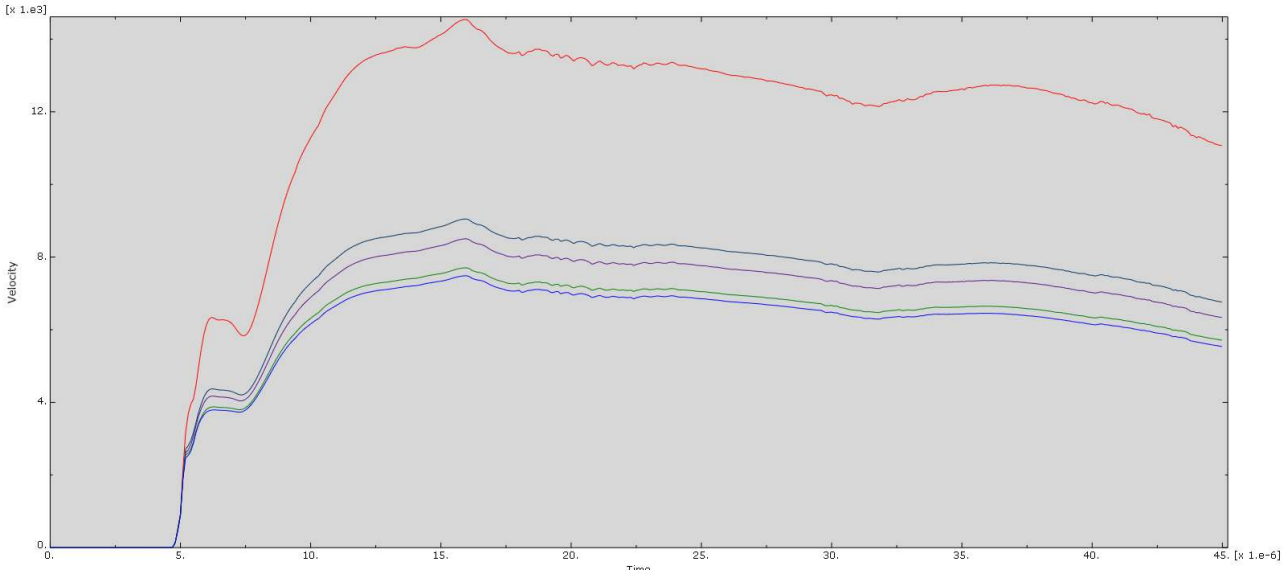

Graph 6 - Titanium liner

The copper liner achieved a maximum velocity of roughly 6E03 m/s (6 km/s) and showed a gradual decline thereafter, while the titanium liner reached a peak

velocity of roughly 8E03 m/s (8 km/s) followed by a much more marked decline in velocity.

Material	Peak jet velocity (km/s)
Copper	6
Titanium	8

Table 7 - Observed jet tip velocity

The chief differences in material properties between copper and titanium are density and melting temperature [41], as shown below:

Material	Density (kg/m^3)	Melting Temperature (K)
Copper	7850	1790
Titanium	4314	1935

Table 8 - Key material differences between copper and titanium

Research has shown that the melting temperature of a material significantly affects the velocity of a shaped charge jet [42] [37], with higher melting temperatures desirable. As titanium has a higher melting temperature than copper, the increased jet velocity observed in the simulations is consistent with the published research.

Research comparing copper and titanium shaped charge liners [38] has found that titanium liners compared favourably to copper, with Bourne et al recording a peak jet tip velocity of 6.46 km/s for titanium and 5.9 km/s for copper. The differences in jet tip velocity observed in the sumulations described in this paper shows good agreement with those described in [38].

7.1.2 Velocity (3D simulation)

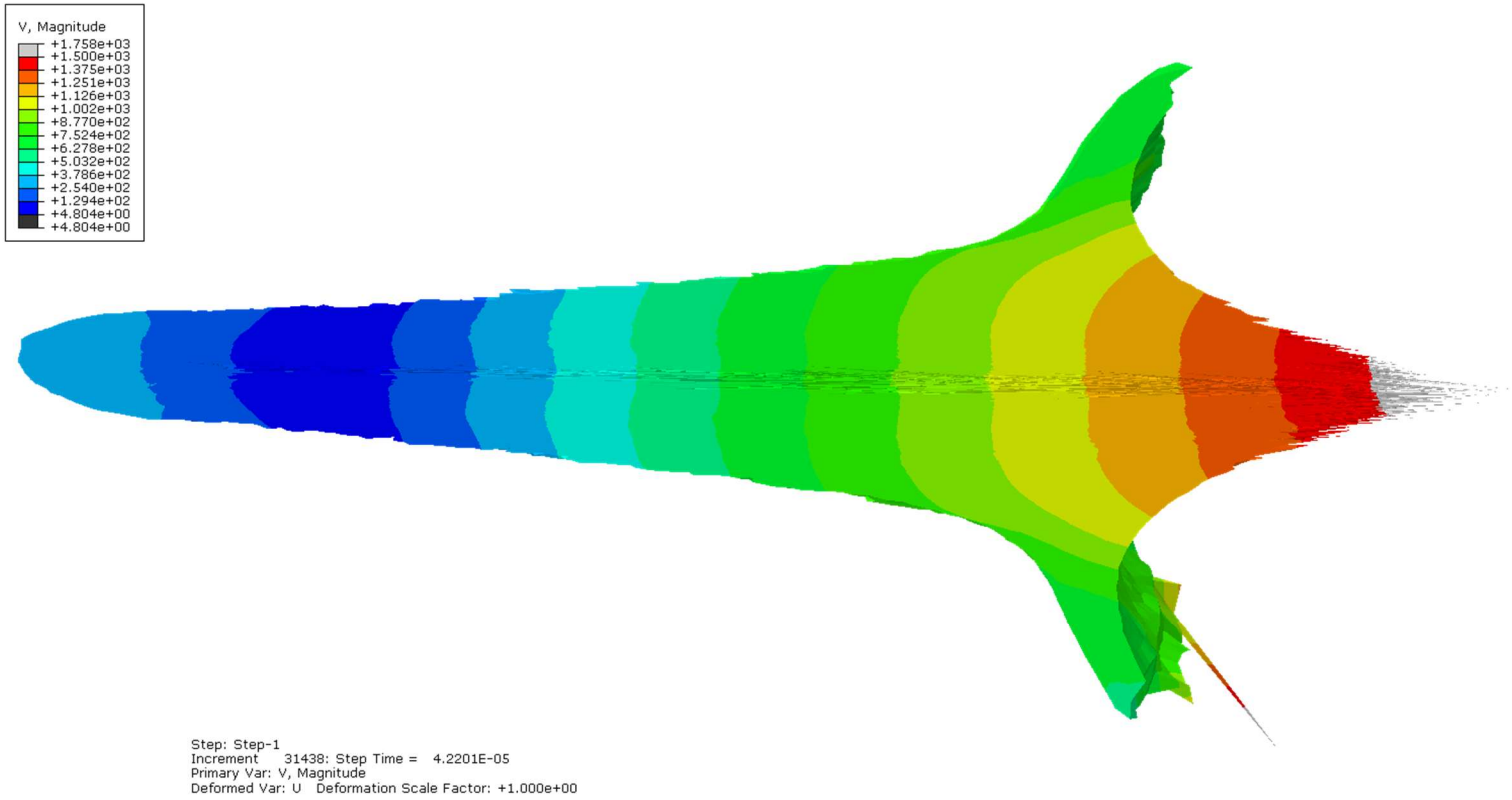

Figure 33 - Velocity of the shaped charge jet (3D simulation)

Figure 28 shows the shape and velocity of the liner at the conclusion of the 3D simulation. While the tip of the jet shows the highest velocities, a gradient can be observed wherein the nodal velocity decreases towards the ‘tail’ of the jet, before increasing again, in the opposite direction. The jet is therefore observed to be ‘stretching’ along the X axis rather than moving in a single direction. This issue was not observed during either of the 2D simulations, and is thought to be an effect of the 3D model created.

It is also possible that the stretching is a stage of the jet formation, and that if the simulation had progressed further a shaped charge jet may have developed fully. However, excessive element distortion within the liner caused the simulations to crash before this could be observed, and attempts to use SPH or ALE to remedy this were unsuccessful.

Jet tip velocity during the 3D simulation remains similar to the 2D simulations, with a rapid acceleration and a brief period of stability followed by a second rapid increase.

8 Conclusion

Shaped charge systems are the focus of significant research and development due to their varied applications within the defence and civilian sector. This research focuses on the refinement of shaped charge designs utilising novel liner shapes, metal alloys and energetic fills in order to maximise the efficiency of specialised designs.

2D simulations of shaped charge systems created in the Abaqus CAE suite featuring copper and titanium liners show good agreement with literature in terms of jet tip velocity. The same design translated into a 3D model described some unexpected behaviour, which may be explained by further experimentation, but demonstrated a similar jet tip velocity curve to that seen in the 2D simulations.

9 Bibliography

[1] W. Walters, *An Overview of the Shaped Charge Concept,* US Military Academy West Point: Mathematical Sciences Centre of Excellence .

[2] D. R. Kennedy, History of the Shaped Charge Effect, Mountain View, California: D. R. Kennedy & Associates, Inc. , 1983.

[3] W. P. Walters and J. A. Zukas, Fundementals of Shaped Charges, New York: John Wiley & Sons, 1989.

[4] J. Norris, Anti-Tank Weapons, Brassey's, 1996.

[5] AMCP 706-290, Engineering Design Handbook, Warheads, General (U), Washington DC: US Army Material Command Headquarters, July 1964.

[6] J. Harvey, B. Grove, L. Zhan and L. Behrmann, “New Predictive Model of Penetration Depth for Oilwell-Perforating Shaped Charges,” in *SPE International Symposium and Exhibition on Formation Damage Control*, Lafayette, Louisiana, 2010.

[7] S. Zhao, Z. Xu, J. Zhong and K. Sun, “The Application of Shaped Charge Blasting Technology in Open-pit Mine,” *Mathematical Modelling of Engineering Problems,* vol. 3, no. 2, pp. 91-95, 2016.

[8] W. P. Walters and J. A. Zukas, Explosive Effects and Applications, New York, NY: Springer, 1998.

[9] H. P. Ma, K. Yi, M. A. Zhou, M. C. Qiu and K. B. Li, “Blasting Technology for Demolition of Large-Scale Steel Structure Buildings by Shaped Charge Cutter,” *Advanced Materials Research,* vol. 594, no. 1, pp. 702-707, 2012.

[10] SAAB Defence Industries, “Carl-Gustaf System,” [Online]. Available: https://www.saab.com/products/carl-gustaf-m4. [Accessed 27 12 2025].

[11] A. H. Menon and D. G. K. Jayaraj, “Comparative Study of Demolition Methods,” *International Journal of Advanced Scientific Research and Engineering Trends,* vol. 2, no. 2, 2017.

[12] M. L. Combrinck, T. Gadal, A. Hargreaves and J. E. Martin, “Velocity Tracking of Shaped Charge Wire Formation and Propogation Towards the Target,” Northumbria University, Department of Mechanical and Construction Engineering, Newcastle-Upon-Tyne.

[13] K. C. Albayrak, M. Ucuncu and F. Elaldi, “Design of Shaped Charges with Optimum Armored Penetration Efficiency,” *Defence Science Journal,* vol. 74, no. 6, pp. 822-833, November 2024.

[14] E. E. El-Sayed, T. A. Elshenawy, M. A. Shaker and A. M. Riad, “Influence of Different Shaped Charge Parameters on Jet Penetration into Metallic Target,” *Journal of Physics, Conference Series,* vol. 2299, 2022.

[15] P. Zhou, R. Li, D. Zhou, T. Liu, M. Wang and Z. Wang, “Design and Experimental Research of a New Shaped Charge Liner for Enhanced Armor Piercing and Lateral Damage,” *Shock and Vibration,* 2024.

[16] H. Shekhar, “Theoretical Modelling of Shaped Charges in the Last Two Decades (1990-2010): A Review,” *Central European Journal of Energetic Materials,* vol. 9, no. 2, pp. 155-185, 2012.

[17] J. Abramson, “West Rushes Weapons to Ukraine,” *Arms Control Today,* vol. 52, no. 3, pp. 29-31, 2022.

[18] R. Fong, W. Ng, B. Rice and S. Tang, “Multiple Explosively Formed Penetrator (MEFP) Warhead Technology Development,” in *19th International Symposium of Ballistics*, Interlaken, Switzerland, 2001.

[19] Belma, “Mina przeciwburtowa z zapalnikiem niekontaktowym MPB-ZN,” [Online]. Available: https://www.belma.pl/wyroby/wyroby-specjalne/systemy-minowania-miny/miny-przeciwburtowe/mina-

przeciwburtowa-z-zapalnikiem-niekontaktowym-mpb-zn. [Accessed 26 11 2025].

[20] Global Security, “M898 SADARM,” [Online]. Available: https://www.globalsecurity.org/military/systems/munitions/sadarm.htm. [Accessed 26 11 2025].

[21] C. Wang, J. Ding and H. Zhao, “Numerical Simulation on Jet Formation of Shaped Charge with Different Liner Materials,” *Defence Science Journal,* vol. 64, no. 4, p. 279, 2015.

[22] S. Fetter and F. N. von Hippel, “The Hazard Posed by Depleted Uranium Munitions,” *Science & Global Security,* vol. 8, no. 2, pp. 125-161, 2007.

[23] E. L. Baker, S. DeFisher, A. Daniels, T. Vuong and J. Pham, “Glass as a Shaped Charge Liner Material,” in *Proceedings of the 26th International Symposium on Ballistics*, 2011.

[24] D. H. Lassiala, “Mechanical Behaviour of Tungsten Shaped Charge Liner Materials,” in *14th International Ballistics Symposium and Exhibition*, Quebec, Canada, 1993.

[25] Z. Huang, Z. Huang and X. Zu, “Study on Dynamic Mechanical Properties of Tungsten Copper Alloy and Application of Shaped Charge,” *Journal of Physics: Conference Series,* 2023.

[26] M. Sun, C. Li, X. Zhang, X. Hu, X. Hu and Y. Liu, “Rectivity and Penetration Performance Ni-Al and Cu-Ni-Al Mixtures as Shaped Charge Liner Materials,” *Materials,* vol. 11, no. 11, 2018.

[27] M. J. Murphy, “The Effect of Gradients in HMX/TNT Content and Porosity on Shaped Charge Jet Characteristics,” in *11th International Symposium on Ballistics*, Brussels, 1989.

[28] Defence Safety Authority, *DSA 03.OME Part 1: Defence Code of Practice 112, OME Vulnerability (Insensitive Munitions) version 1.1,* August 2024.

[29] M. Ahmed, Z. Xiang Huang, A. Malik, X. D. Zu, Q. Q. Xiao and M. Ahmed, “Penetration Performance of Shaped Charge Jets Using Insensitive Munitions: Simulative and Experimental Studies,” *Advanced Materials Research,* vol. 1102, no. 1, pp. 119-123, May 2015.

[30] Y. Voitenko, Y. Sydorenko, R. Zakusylo, S. Goshovskii, S. Zaichenko and V. Boyko, “On the Influence of Liner Shape and Charge Detonation Scheme on the Kinetic Characteristics of Shaped Charge Jets and Explosively Formed Penetrators,” *Central European Journal of Energetic Materials,* vol. 20, no. 4, pp. 417-441, 2023.

[31] M. Cartwright, D. Lloyd-Roach and P. J. Simpson, “Non-Solid Explosives for Shaped Charges. Part II. Target Penetration with Metal Liner Devices Using Sensitized Nitromethane Liquid Explosive,” *Journal of Energetic Materials,* vol. 27, no. 3, 2009.

[32] H. Shekhar, “Explosive Characteristics and Shaped Charge Applications of Nitromethane (NM): A Review,” *Central European Journal of Energetic Materials,* vol. 9, no. 1, pp. 87-97, 2012.

[33] E. Predang, M. Markovic, D. Jevtic and R. Durovic, “Modeling of Shaped Charge Jet Penetration Depth: Analytical and Numerical Approach,” *Scientific Technical Review,* vol. 74, no. 2, pp. 17-22, 2024.

[34] K. T. Miers, N. P. Peterson, W. L. Perry, L. A. Lystrom, J. C. Sweitzer and S. E. DeFisher, “Modeling and Analysis of a 66 mm Shaped Charge,” *International Journal of Impact Engineering,* vol. 206, no. 1, 2025.

[35] Dassault Systemes, “Abaqus/CAE,” [Online]. Available: https://www.3ds.com/products/simulia/abaqus/cae. [Accessed 02 12 2025].

[36] Y. Gocmen, C. Erdogan and T. Yalcinkaya, “A Numerical Study on the Ballistic Performance of Projectiles Formed by Shaped Charge,” *Journal of Applied Mechanics,* vol. 90, no. 11, 2023.

[37] A. Catovic, “Research of Influence of Different Shaped Charge Liner Materials on Penetration Depth Using Numerical Simulations,” *Periodicals of Engineering and Natural Sciences,* vol. 22, no. 4, pp. 1-26, 2023.

[38] B. Bourne, K. G. Cowan and J. P. Curtis, “Shaped Charge Warheads Containing Low Melt Energy Metal Liners,” in *19th International Symposium on Ballistics*, 2001.

[39] G. R. Johnson and W. H. Cook, “A Constitutive Model and Data for Metals Subjected to Large Strains, High Strain Rates and High Temperatures,” in *Proceedings of the 7th International Symposium on Ballistics*, The Hague, 1983.

[40] E. L. Lee, H. C. Hornig and J. W. Kury, Adiabatic Expansion of High Explosive Detonation Products, UCRL-50422, 1968.

[41] ANSYS Inc, *AUTODYN material library.*

[42] J. Shi, Z.-x. Huang, X.-d. Zu and Q.-q. Xiao, “Experimental and Numberical Investigation of Jet Performance Based on Johnson-Cook Model of Liner Material,” *International Journal of Impact Engineering,* vol. 170, 2022.

[43] Q. Xiao, Z. Huang, X. Zu, X. Jia and B. Ma, “The Effects of Compressibility and Target Strength on Shaped Charge Jet Penetration,” *Defence Technology,* 2025.